

1 **Sensitivity of simulated global-scale freshwater fluxes and**  
2 **storages to input data, hydrological model structure,**  
3 **human water use and calibration**

4  
5 **H. Müller Schmied<sup>1</sup>, S. Eisner<sup>2</sup>, D. Franz<sup>3\*</sup>, M. Wattenbach<sup>3</sup>, F. T. Portmann<sup>1,4,5</sup>,**  
6 **M. Flörke<sup>2</sup> and P. Döll<sup>1</sup>**

7 [1]{Institute of Physical Geography, Goethe-University Frankfurt, Altenhöferallee 1, 60438  
8 Frankfurt am Main, Germany}

9 [2]{Center for Environmental Systems Research (CESR), University of Kassel,  
10 Wilhelmshöher Allee 47, 34117 Kassel, Germany}

11 [3]{GFZ German Research Centre for Geosciences, Section 5.4 Hydrology, Telegrafenberg,  
12 14473 Potsdam, Germany}

13 [4]{Biodiversity and Climate Research Centre (LOEWE BiK-F), Senckenberganlage 25,  
14 60325, Frankfurt am Main, Germany}

15 [5]{Senckenberg Research Institute and Natural History Museum, Senckenberganlage 25,  
16 60325, Frankfurt am Main, Germany}

17 \* now at Inorganic and Isotope Geochemistry, GFZ Potsdam

18  
19 Correspondence to: H. Müller Schmied ([hannes.mueller.schmied@em.uni-frankfurt.de](mailto:hannes.mueller.schmied@em.uni-frankfurt.de))

## 1 **Abstract**

2 Global-scale assessments of freshwater fluxes and storages by hydrological models under  
3 historic climate conditions are subject to a variety of uncertainties. Using the global  
4 hydrological model WaterGAP 2.2, we investigated the sensitivity of simulated freshwater  
5 fluxes and water storage variations to five major sources of uncertainty: climate forcing, land  
6 cover input, model structure/refinements, consideration of human water use and calibration  
7 (or no calibration) against observed mean river discharge. In a modelling experiment, five  
8 variants of the standard version of WaterGAP 2.2 were generated that differed from the  
9 standard version only regarding the investigated source of uncertainty. The basin-specific  
10 calibration approach for WaterGAP was found to have the largest effect on grid cell fluxes as  
11 well as on global AET and discharge into oceans for the period 1971-2000. Regarding grid  
12 cell fluxes, climate forcing ranks second before land cover input. Global water storage trends  
13 are most sensitive to model refinements (mainly modelling of groundwater depletion) and  
14 consideration of human water use. The best fit to observed time series of monthly river  
15 discharge or discharge seasonality is obtained with the standard WaterGAP 2.2 model version  
16 which is calibrated and driven by daily observation-based WFD/WFDEI climate data.  
17 Discharge computed by a calibrated model version using monthly CRU 3.2 and GPCC v6  
18 climate input reduced the fit to observed discharge for most stations. Taking into account  
19 uncertainties of climate and land cover data, global 1971-2000 discharge into oceans and  
20 inland sinks ranges between 40 000 and 42 000 km<sup>3</sup> yr<sup>-1</sup>. Global actual evapotranspiration,  
21 with 70 000 km<sup>3</sup> yr<sup>-1</sup>, is rather unaffected by climate and land cover uncertainties. Human  
22 water use reduced river discharge by 1000 km<sup>3</sup> yr<sup>-1</sup>, such that global renewable water  
23 resources are estimated to range between 41 000 and 43 000 km<sup>3</sup> yr<sup>-1</sup>. The climate data sets  
24 WFD (available until 2001) and WFDEI (starting in 1979) were found to be inconsistent with  
25 respect to short wave radiation data, resulting in strongly different actual evapotranspiration.  
26 Global assessments of freshwater fluxes and storages would therefore benefit from the  
27 development of a global data set of consistent daily climate forcing from 1900 to current.

28

29

30

31

## 1 **1 Introduction**

2 The quantification of global scale freshwater fluxes, in particular river discharge, is essential  
3 to assess availability and scarcity of water resources for humans and the environment for both  
4 present (Hoekstra et al., 2012; Oki and Kanae, 2006; Prudhomme et al., 2014) and scenario  
5 conditions (Döll and Müller Schmied, 2012; Masaki et al., 2014; Schewe et al., 2014). Further  
6 examples are the estimation of amounts and spatial distribution of precipitation (Harris et al.,  
7 2014; Schneider et al., 2014) and evapotranspiration (Jasechko et al., 2013; Jung et al., 2010;  
8 Sterling et al., 2012). As groundwater plays an important role for humans e.g. for irrigation  
9 purposes, related fluxes such as groundwater recharge (Döll and Fiedler, 2008; Koiraala et al.,  
10 2014; Portmann et al., 2013) or, as consequence of an overexploitation of groundwater  
11 resources, groundwater depletion (Döll et al., 2014, Wada et al., 2010) are focus of modeling  
12 activities.

13 These examples show attempts to quantify global scale freshwater fluxes as well as water  
14 storages however the methodologies used differ largely. Interpolation of in-situ measurements  
15 works well with a dense monitoring network. Hence, precipitation products (e.g. GPCP  
16 (Schneider et al., 2014), CRU (Harris et al., 2014)) are often based solely on interpolation of  
17 station data. In combination with other data sources like remote sensing, even less dense point  
18 measurements are used, e.g. to quantify global evapotranspiration (Jung et al., 2010). In  
19 particular, remote sensing is used to derive spatio-temporal input data for evapotranspiration  
20 schemes (Miralles et al., 2011; Vinukollu et al., 2011; Wang and Liang, 2008) or to assess  
21 total continental water storage variations (Schmidt et al., 2006). Spatio-temporal patterns of  
22 consistent multiple fluxes and storages can be obtained using land surface models (LSMs) and  
23 global hydrological models (GHMs). LSMs, which have evolved as “land components” of  
24 Global Circulation Models (GCMs), usually have a high temporal resolution and solve the  
25 energy balance (Haddeland et al., 2011). However, they do have limitations, esp. in runoff  
26 routing and with regard to human alterations of the water cycle (even though there are  
27 exceptions, e.g. Pokhrel et al. (2012)). GHMs are explicitly designed to assess the state of  
28 freshwater resources and to address water-related problems like floods and droughts (Corzo  
29 Perez et al., 2011; Prudhomme et al., 2011) and human impacts on freshwater resources. In  
30 the last 20 years, a number of GHMs have been developed using different conceptual  
31 approaches, e.g. VIC (Nijssen et al., 2001), WBM (Vörösmarty et al., 1998), Mac-PDM  
32 (Gosling and Arnell, 2011), WASMOD-M (Widén-Nilsson et al., 2007), H08 (Hanasaki et al.,

1 2008), Water – Global Assessment and Prognosis (WaterGAP) (Alcamo et al., 2003; Döll et  
2 al., 2003) and PCR-GLOBWB (Sperna Weiland et al., 2010).

3 Freshwater fluxes and storages simulated by GHMs and LSMs are subject to several sources  
4 of uncertainty: spatially distributed input data (e.g. climate forcing, water use, land cover),  
5 model structure (or modeling approach) and model parameters. In addition, epistemic  
6 uncertainty due to a lack of knowledge and understanding of processes is of particular  
7 importance at the global scale (see discussion in Beven and Cloke (2012) and Wood et al.  
8 (2011, 2012)).

9 Uncertainties due to the choice of climate forcing were the focus of few studies. For example,  
10 Guo et al. (2006) showed the large sensitivity of soil moisture simulated by 11 LSMs to  
11 different climate forcing data sets (esp. to precipitation and radiation). They concluded that  
12 this uncertainty associated with land surface hydrology is as large as the variation among the  
13 LSMs. Biemans et al. (2009) evaluated seven global precipitation products for 294 river  
14 basins worldwide and quantified an average uncertainty of 30% per basin. They studied the  
15 dynamic global vegetation and hydrology model LPJmL (Bondeau et al., 2007) with these  
16 precipitation forcings. As consequence of the large spread of precipitation input, discharge  
17 uncertainty was quantified with about 90%. Even though climate forcing is of such  
18 importance, only few studies are available which study the uncertainty in a global  
19 hydrological model setup.

20 Uncertainties in terms of model structure are related to the design of the model, i.e. the  
21 processes considered and their representation by conceptual approaches. To consider this kind  
22 of uncertainty, Butts et al. (2004); Clark et al. (2008); Refsgaard et al. (2006) and Song et al.  
23 (2011) developed approaches to diagnose different structures of hydrological models and  
24 related uncertainties. The model intercomparison efforts WATCH WaterMIP (Haddeland et  
25 al., 2011) and ISI-MIP (Warszawski, et al., 2013) have shown the effects of different model  
26 structures (Gudmundsson et al., 2012a, 2012b; Hagemann et al., 2013; Van Loon et al., 2012;  
27 Prudhomme et al., 2014; Schewe et al., 2014) even though this was not explored  
28 systematically. For example, values for global annual evapotranspiration between 60 000 and  
29 85 000 km<sup>3</sup> yr<sup>-1</sup> were reported in the WATCH WaterMIP study (Haddeland et al., 2011). In  
30 such multi-model studies, many completely different models are participating, which makes it  
31 very difficult to identify the reasons for different model behavior. A sensitivity study using

1 basically the same model but with a refined model structure can therefore be of benefit (e.g.  
2 Thompson et al., 2013).

3 Model parameters are used to represent system dynamics in solvable equations, in particular  
4 when the hydrological process cannot be described physically. These parameters are generally  
5 not measurable and, hence, are a source of uncertainty that can influence model results to  
6 varying degrees. Within the GCM community, the perturbed physics ensemble approach has  
7 been used to assess this kind of uncertainty in a structured way (Collins et al., 2006;  
8 Rowlands et al., 2012). Global scale hydrology applications also assess parameter uncertainty.  
9 For example, Gosling and Arnell (2011) used seven sets of parameter perturbations for two  
10 model parameters of the GHM Mac-PDF.09. For the GHM WaterGAP, Kaspar (2003)  
11 investigated the impact of uncertainty of 38 model parameters on simulated river discharge by  
12 conducting various model runs with a sampling of parameter values within specific ranges.  
13 He found that major uncertainties are related to evapotranspiration parameters and land cover  
14 specific attributes. Schumacher et al. (2014) confirmed the sensitivity of model output (here:  
15 monthly total water storage) to radiation calculation and related parameters in WaterGAP  
16 which, together with a river roughness coefficient and precipitation, dominate uncertainty in  
17 many of the 33 investigated river basins. Groundwater-related parameters and soil parameters  
18 were found to be important for the timing and variation of total water storages in WaterGAP  
19 (Werth and Güntner, 2010).

20 Model parameters can be adjusted by calibration, such that model output matches an observed  
21 set of data. Whereas basin-scale hydrological models are routinely calibrated against observed  
22 river discharge (e.g. Beven, 2001), this is only seldom the case for GHMs. Widén-Nilsson et  
23 al. (2007) used different model parameter sets within the GHM WASMOD-M to define  
24 optimal parameter values on river basin scale. WaterGAP is calibrated against observed river  
25 discharge in a basin-specific manner by varying one soil parameter (and up to two correction  
26 factors) (Döll et al., 2003; Hunger and Döll, 2008).

27 In this paper, we analyze and quantify the uncertainty in global-scale simulated freshwater  
28 water fluxes and storages due to 1) spatially distributed input data, and 2) model structure and  
29 modeling approach, using the most recent version of the GHM WaterGAP 2.2. Previous  
30 studies (Kaspar, 2003; Schumacher et al., 2014; Werth and Güntner, 2010) have already  
31 investigated both parameter sensitivity and uncertainty for WaterGAP. To assess recently

1 available climate forcing and land cover input data as well as significant modifications of  
2 WaterGAP model structure during the last decade were major motivations of this experiment.

3 In particular, we will answer the following research questions:

4 i) How sensitive are freshwater fluxes and water storages to spatially distributed input  
5 data (climate forcing, land cover)?

6 ii) What are the benefits of WaterGAP model structure refinements implemented during  
7 the last decade?

8 iii) How does the modeling approach (calibration procedure, consideration of human  
9 water use) affect freshwater fluxes and water storages?

10 iv) Which type of uncertainty is dominant for specific fluxes and variations of total water  
11 storage?

12 After an initial description of WaterGAP 2.2 (for details see the Appendix), the experimental  
13 setup is explained (Sect. 2). In Sect. 3, the results are described; focusing on the effect of the  
14 different model variants on global freshwater fluxes and water storages as well as spatial  
15 patterns. In Sect. 4, we discuss the results with regard to the research questions. The paper  
16 ends with a summary and conclusions (Sect. 5).

17

## 18 **2 Methods and experiment setup**

### 19 **2.1 Description of WaterGAP 2.2**

20 The global hydrology and water use model WaterGAP (Fig. 1) consists of two major parts,  
21 the water use models for five different sectors (Appendix C) and the WaterGAP Global  
22 Hydrology Model (WGHM, Fig. A1). The submodel GroundWater-Surface-Water-USE  
23 (GWSWUSE) (Appendix D) is used to distinguish water use from groundwater and surface  
24 water sources and computes net abstractions from both sources which are an input to WGHM  
25 (Fig. 1). Using a number of water storage equations (change of storage over time equals to  
26 inflow minus outflows, Appendix A), WGHM calculates daily water flows and storages at a  
27 spatial resolution of  $0.5^\circ$  by  $0.5^\circ$  (55 km by 55 km at the equator) for the whole land area of  
28 the Earth except Antarctica (66896 cells). WaterGAP 2.2 is calibrated against mean annual

1 river discharge at 1319 gauging stations, and the adjusted calibration factor is regionalized to  
2 grid cells outside the calibration basins (Appendix B).

3 Since the initial publication of WaterGAP 2.1d (Döll et al., 2003), major changes were made  
4 to keep the model up-to-date. For example, algorithms of reservoir operation were included  
5 (Döll et al., 2009), groundwater recharge was optimized by distinguishing semi-arid / arid  
6 regions from humid regions (Döll and Fiedler, 2008), a variable flow velocity algorithm was  
7 included (Verzano et al., 2012) and the source of abstracted water was considered (Döll et al.,  
8 2012).

## 9 **2.2 Experiment setup**

10 Six WaterGAP model variants (Table 1) were designed as follows. The standard version of  
11 WaterGAP 2.2 (STANDARD) was modified regarding only one aspect, including either  
12 alternative climate forcing (CLIMATE), land cover input (LANDCOVER) or model structure  
13 (STRUCTURE). Each model variant was independently calibrated. Variant NoCal is an  
14 uncalibrated simulation with the standard version of WaterGAP 2.2 to study the impact of the  
15 calibration approach. Variant NoUse reflects naturalized water flows and storages without the  
16 impact of human water use, and thus also renewable water resources.

17 In addition, for assessing the effect of uncertainties on renewable water resources, variants  
18 CLIMATE, LANDCOVER, STRUCTURE and NoCal are also run without considering any  
19 water abstractions. The simulation period is 1901-2009 but model results are evaluated only  
20 for 1971-2000.

### 21 **2.2.1 Climate input**

22 Climate forcing data for global scale hydrological models are a major source of uncertainty  
23 for two main reasons: (1) they are subject to measurement errors which were not corrected in  
24 the original input data and (2) they are subject to interpolation errors due to low spatial and  
25 temporal monitoring network density and/or because (temporal) data gaps have to be filled.  
26 To analyze the sensitivity of calibration and simulated freshwater fluxes to different climate  
27 forcing datasets, two climate forcings were used to force both WGHM and the Global  
28 Irrigation Model GIM (Döll and Siebert, 2002) (Appendix C).

29 In variant STANDARD, the daily WATCH Forcing Data methodology applied to ERA-40  
30 data (WFD) (Weedon et al., 2011) for the years 1901 to 1978 (the years 1901 to 1957 are

1 based on reordered reanalysis data) and the WATCH Forcing Data methodology applied to  
2 ERA-Interim data (WFDEI) (Dee et al., 2011; Weedon et al., 2010, 2011) for the years 1979  
3 to 2009 was chosen. Switching the climate input dataset in 1979 leads to inconsistencies in  
4 terms of AET (higher in WFDEI) and therefore affects the storages until a new equilibrium is  
5 reached (see Sect. 3.1). WFD and WFDEI monthly sums/means are bias-corrected with other  
6 data sources (temperature bias correction, shortwave radiation adjustment using cloud cover  
7 and adjustment of number of wet days to CRU TS 2.1 for WFD and to CRU TS 3.1 for  
8 WFDEI as well as adjustment of monthly precipitation sum to GPCC v4 (WFD) and GPCC  
9 v5 (WFDEI) and snowfall undercatch corrected after Adam and Lettenmaier (2003)). To  
10 calculate net shortwave radiation, the incoming shortwave radiation is reflected by literature  
11 based land cover specific albedo values (see Table A2). Literature based emissivity values for  
12 all land cover classes (Wilber et al., 1999) and the Stefan-Boltzmann-equation are used to  
13 calculate outgoing longwave radiation. The difference to incoming longwave radiation  
14 represents net longwave radiation. Net radiation is the sum of both components.

15 In variant CLIMATE, the monthly dataset CRU TS 3.2 (Harris et al., 2014) was used but  
16 monthly precipitation totals were replaced by the latest GPCC v6 precipitation monitoring  
17 product (Schneider et al., 2014) because it includes more observation stations. Monthly means  
18 are disaggregated to daily values within WaterGAP (Döll et al., 2003). Neither CRU nor  
19 GPCC precipitation is corrected for observational errors, e.g. wind induced precipitation  
20 undercatch. Thus, Döll and Fiedler (2008) included the catch ratios of Adam and Lettenmaier  
21 (2003) and used the empirical function of Legates (1987) to correct especially snow  
22 undercatch by dividing snow and liquid precipitation using a temperature based approach.  
23 The correction of precipitation measurement bias leads to an average increase of 8.7%  
24 compared to the original product. On 37.5% of the land area (except Greenland and  
25 Antarctica), the increase of precipitation is larger than 10%. Differences of mean values from  
26 both datasets (CRU/GPCC and WFD/WFDEI) occur due to the slightly different precipitation  
27 correction approach and the GPCC version used for scaling monthly sums. Monthly  
28 precipitation is equally distributed to the number of wet days provided by the CRU 3.2  
29 dataset; the distribution of wet days within a month is modeled as a two-state, first-order  
30 Markov chain (Döll et al., 2003). Cloudiness fraction was used to calculate incoming short  
31 wave radiation as well as outgoing long wave radiation after Shuttleworth (1993), see also  
32 Döll et al. (2003).



## 1 2.2.2 Land cover input data

2 The distribution of land cover classes and associated attributes are affecting simulated fluxes  
3 in terms of radiation energy balance (albedo and emissivity), snow dynamics (degree-day  
4 factor  $D_F$ ), available soil water capacity (rooting depth) and interception capacity ( $L$ ) (for  
5 details see Appendix A). To estimate the effect of different, homogeneous-source land cover  
6 data, two input maps were used (Fig. 2). Attributes and model parameters associated to land  
7 cover classes were derived from literature or previous model versions (Table A2) and left  
8 equal in both variants.

9 In variant STANDARD we used the gridded MODIS (Moderate-resolution Imaging  
10 Spectroradiometer) land cover product (MOD12Q1) for the year 2004. The product  
11 MOD12Q1 (1 km resolution, global coverage up to 80° N) was used with land cover type 1  
12 according to the International Geosphere-Biosphere Programme (IGBP) classification. After  
13 resampling to 0.5° spatial resolution, the dataset was reclassified to fit to the WaterGAP land  
14 cover classification system (Table A2). As water bodies (from the global lakes and wetlands  
15 database, GLWD (Lehner and Döll, 2004)) and percentage of urban area (from previous  
16 model versions) are obtained by additional input files, the second land cover class was  
17 appointed in case of “water” or “urban and built-up” as primary land cover. For coastal grid  
18 cells which are not fully covered by MODIS and north of 80° N, a combination of Global  
19 Land Cover Characteristics database GLCC (USGS, 2008) + CORINE land cover information  
20 was used.

21 In variant LANDCOVER, a combination of the GLCC based on the years 1992/1993 and, for  
22 Europe, CORINE Land Cover based on the year 2000 (European Environment Agency, 2004)  
23 was used as land cover information, as also in a previous WaterGAP version (Haddeland et  
24 al., 2011). The idea was to use an IGBP based classification scheme and a remote sensing  
25 based land cover distribution instead of IMAGE (Alcamo et al., 1998) model outputs (as in  
26 previous model versions). Both input datasets have a resolution of 1 by 1 km and were  
27 aggregated to the 0.5° model resolution by assigning the majority land cover type.

## 28 2.2.3 Structural model changes

29 During the last 10 years, the WaterGAP model was subject to several revisions and  
30 improvements in terms of hydrologic process representation, resulting in an overall more  
31 complex model structure. To assess the sensitivity of simulated freshwater fluxes to model

1 complexity, one model variant with a simplified structure comparable to Döll et al. (2003)  
2 (variant STRUCTURE) was set up which was run with the same input data as all other model  
3 variants. Differences of variant STRUCTURE as compared to the other variants are as  
4 follows.

- 5 • Flow velocity is globally set to  $1 \text{ m s}^{-1}$  and the meandering ratio is set to 1, instead of  
6 the variable flow velocity algorithm of Verzano et al. (2012) in the other variants.
- 7 • Reservoirs are treated as global lakes, i.e. the reservoir operation algorithm of Döll et  
8 al. (2009) is not used, which should result in a more dynamic discharge downstream of  
9 reservoirs.
- 10 • Water for human water use is abstracted only from surface water bodies, i.e. there are  
11 no groundwater abstractions as introduced by Döll et al. (2012).
- 12 • Evaporation from lakes/wetlands is not adjusted by reduction factors (Hunger and  
13 Döll, 2008) resulting in evaporation at potential rate even at low storage.
- 14 • Snow accumulation and melt are modeled on  $0.5^\circ$  (instead of the 3 arc minute sub-grid  
15 (Schulze and Döll, 2004)) which should lead to less snow dynamics.
- 16 • Finally, there is no distinction in groundwater recharge for semi-arid / arid and humid  
17 regions (in contrast to Döll and Fiedler (2008) all regions are treated like humid  
18 regions) resulting in higher groundwater recharge in semi-arid / arid regions.

#### 19 2.2.4 Human water use

20 In many areas of the globe, human water use significantly affects water flows and storage. In  
21 this experiment, all model variants except NoUse and STRUCTURE are taking into account  
22 water use from surface water and groundwater resources. In variant NoUse it is assumed that  
23 there are no water abstractions at all, while in STRUCTURE, water is only abstracted from  
24 surface water (as formerly no information on the source of water abstractions was available).

#### 25 2.2.5 Calibration

26 WGHM is calibrated against mean annual discharge in a basin-specific manner by adjusting a  
27 runoff coefficient that affects the outflow from the soil compartment in each grid cell of the  
28 1319 calibration basins. If necessary to simulate mean annual discharge within 1% of the  
29 observed value, two additional correction factors are adjusted (for details see Appendix B).

1 All other parameters are globally uniform (or land cover class dependent), based on literature  
2 or experiences from past studies, i.e. there is no basin or region specific modification. All  
3 model variants except NoCal are independently calibrated to the same observational data. In  
4 variant NoCal, the runoff coefficient and both corrections factors are set to 1 in all grid cells.  
5 The comparison of NoCal to e.g. STANDARD allows for a direct quantification of the effect  
6 of calibration on simulated water fluxes and storages.

## 7 **3 Results**

### 8 **3.1 Global water balance**

9 Table 2 lists global values for various components of the global water balance and changes in  
10 total water storages (TWS) (calculated excluding Antarctica, Greenland and inland sinks) as  
11 estimated by the different model variants. Global values vary mainly due to calibration and  
12 selected climate forcing. For interpreting Table 2 and Figure 3 it is important to mention that  
13 actual evapotranspiration (AET) does not include additional evapotranspiration caused by  
14 irrigation and other human water use. This part of evapotranspiration is called actual water  
15 consumption ( $WC_a$ ). For computing global values of AET and renewable water resources  
16 (RWR), the values were adjusted in calibration basins using the station correction factor CFS  
17 such that a closed global water balance is achieved (for calibration details see Appendix B).  
18 Grid cell values of AET and RWR (Figs. 3 and 4), however, do not reflect CFS to avoid  
19 physically implausible values that likely result from inconsistencies between precipitation  
20 data and observed river discharge. Global precipitation  $P$  is about  $1900 \text{ km}^3 \text{ yr}^{-1}$  (or 1.7%)  
21 higher when using the CLIMATE model variant which results in an equal increase of  
22 discharge compared to STANDARD. Except for NoCal, global AET (calculated as sum of  
23  $E_c$ ,  $E_{sn}$ ,  $E_s$  and  $E_w$ , see Appendix A) does not vary considerably among the variants. In  
24 general, discharge to oceans and inland sinks is lower by the amount of change in AET.  $WC_a$   
25 (row 4 in Table 2) varies due to the demand of surface water abstractions and groundwater  
26 abstractions (which differs in CLIMATE due to the forcing of GIM (Appendix C) and in  
27 STRUCTURE where water demand is entirely extracted from surface water resources) and  
28 due to the different water availability for abstractions. In all cases, a large share of the total  
29 water demand could be satisfied (between 90% in STRUCTURE and 96% in CLIMATE).  
30 When human water use is not taken into account (NoUse), AET increases by  $131 \text{ km}^3 \text{ yr}^{-1}$   
31 because evaporation from open water bodies increases as they are not depleted by water uses

1 and additional evapotranspiration of irrigated crops is not included in AET (but quantified  
2 within  $WC_a$ , row 4 in Table 2). As expected, river discharge is higher (by  $758 \text{ km}^3 \text{ yr}^{-1}$ ) in  
3 NoUse. Changes in total water storages ( $142 \text{ km}^3 \text{ yr}^{-1}$  less storage decrease) are also visible,  
4 especially due to no groundwater withdrawals in this variant (Table 3). The sum of these  
5 differences between STANDARD and NoUse is  $1031 \text{ km}^3 \text{ yr}^{-1}$  which equals to  $WC_a$  (row 4  
6 for STANDARD in Table 2).

7 The calibration has a strong effect on freshwater fluxes. Global discharge to oceans and inland  
8 sinks (Q) in NoCal is about  $6400 \text{ km}^3 \text{ yr}^{-1}$  (or 15.7%) higher than in STANDARD, meaning  
9 that the main effect of calibration is lowering discharge. In many river basins, the calibration  
10 parameter  $\gamma$  is higher than the value 1.0 globally used in NoCal which reduces the share of  
11 effective precipitation actually contributing to runoff. Consequently, AET is lower by nearly  
12 the same amount.

13 When comparing CLIMATE to STANDARD, P and Q are both increased by around 1900  
14  $\text{km}^3 \text{ yr}^{-1}$  whereas global AET sums are nearly equal. Most additional Q (1546 of overall 1906  
15  $\text{km}^3 \text{ yr}^{-1}$ ) is generated in non-calibrated grid cells mostly because of an increased P (which  
16 explains 1200 of the additional  $1546 \text{ km}^3 \text{ yr}^{-1}$ ) and a reduced AET (which explains 282 of the  
17 additional  $1546 \text{ km}^3 \text{ yr}^{-1}$ ) in these grid cells.

18 RWR equal long term averaged discharge to oceans and inland sinks (Q in Table 2) but  
19 without considering human water withdrawals. For the STANDARD model variant, RWR are  
20 1.9% higher than with  $WC_a$  (row 3 in Table 2, col NoUse and STANDARD). Q of the other  
21 model variants and hence RWR increase about a similar value (NoCal 2.0%, LANDCOVER  
22 and STRUCTURE 1.9%, CLIMATE 1.6%; values not shown in Table 2).

23 The decreasing trends of total water storage are mainly caused by groundwater depletion,  
24 except in variants NoUse and STRUCTURE where no groundwater abstraction is modeled.  
25 Interestingly, NoCal shows a smaller decrease in groundwater storage than STRUCTURE.  
26 This is also due to the calibration parameter  $\gamma$  which is on average lower in case of NoCal.  
27 The lower  $\gamma$ , the more water leaves the soil and can subsequently contribute to groundwater  
28 recharge. Note that water abstractions from groundwater are taken directly from the  
29 groundwater storage and also return flows are added directly to groundwater storage (without  
30 passing the soil compartment). Hence, there is no difference in soil water storage between  
31 STANDARD and NoUse (Table 3).

1 Except for groundwater and snow, CLIMATE shows less storage depletion than all other  
2 variants that are forced by WFD/WFDEI (Table 3). The strong decrease in case of  
3 WFD/WFDEI is an artifact caused by combining WFD before 1979 with WFDEI after 1979.  
4 With WFDEI that is based on ERA-Interim, AET is around  $70\,000\text{ km}^3\text{ yr}^{-1}$ , compared to  $65$   
5  $000\text{ km}^3\text{ yr}^{-1}$  in case of WFD. This is caused by differences in the shortwave downward  
6 radiation (much higher in WFDEI) which impacts the net radiation as main input for  
7 calculating potential evapotranspiration after Priestley and Taylor (1972). As all model runs  
8 are started in 1901, the storages are more or less in equilibrium until 1978. AET is increased  
9 in the following 22 years by ca. 10% which leads to a higher water loss and therefore to a  
10 reduction of all storage compartments. For all storages except snow, reservoirs and  
11 groundwater, a new equilibrium is achieved a few (around five) years after 1979 on a lower  
12 level (STANDARD variant). Whereas snow storage is not influenced at all, groundwater  
13 storage is affected by groundwater depletion and reservoirs by water use and obvious  
14 limitations of the reservoir algorithm. Thus, an equilibrium is not reached in global average of  
15 the latter two storages but decreasing since 1901.

### 16 **3.2 Actual evapotranspiration**

17 Mean AET shows the highest values around the equator consistent with available energy,  
18 except for the Pacific Rim of South America (Fig. 3a). Among the variants, the largest  
19 differences to STANDARD occur in case of the uncalibrated version NoCal (Fig. 3f). As the  
20 calibration approach also affects grid cells outside of the 1319 calibration basins due to the  
21 regionalization (Appendix B3), all grid cells are affected. In most regions, calibration leads to  
22 higher AET but in the upstream Amazon, the Congo, Arctic river basins and some other  
23 basins, the opposite is true. The global sum of AET of NoCal is 9.2% lower than estimated  
24 with STANDARD (Table 2). Notable differences in AET also occur when using an  
25 alternative climate input (Fig. 3b). AET increases in CLIMATE on 42.6% of the land surface  
26 by more than  $10\text{ mm yr}^{-1}$  and decreases by more than  $10\text{ mm yr}^{-1}$  on 30.5% of the land  
27 surface. It increases (decreases) by more than  $100\text{ mm yr}^{-1}$  on 5.4% (5.6%) of the land surface.  
28 When summed globally, only minor changes in AET occur in case of CLIMATE (increase of  
29 0.06% or  $39\text{ km}^3\text{ yr}^{-1}$ , Table 2). In contrast, AET differences of the STRUCTURE variant are  
30 higher for the global sum (increase of 0.6% or  $414\text{ km}^3\text{ yr}^{-1}$ ) but occur on an overall smaller  
31 area (increase by more than  $10\text{ mm yr}^{-1}$  on 11.9% of the land surface, decrease on 14.2%).  
32 The effect of STRUCTURE is visible in areas with surface water bodies and in snow-

1 dominated areas. On the one hand, an increase in net radiation in snowy regions leads to a  
2 slight increase of AET but in small absolute numbers as total AET is comparatively low. On  
3 the other hand, effects due to the evaporation reduction factor for surface water bodies are  
4 visible. In all variants except STRUCTURE, evaporation is limited when the surface water  
5 body storage is reduced to mimic the shrinking of surface area. Hence, in regions with a high  
6 percentage / volume of surface water bodies, AET is increased. In addition, more complex  
7 effects occur. The Great Lakes, for example, evaporate with potential evapotranspiration PET  
8 in STRUCTURE, even when the lake storage is relatively low. This results in a relatively low  
9 modeled discharge which fits well to the observed ones. Hence, no correction factor (neither  
10 CFA nor CFS) is required in the Great Lakes basin. However, in STANDARD, the reduction  
11 factor reduces evaporation by up to  $\frac{3}{4}$  of PET. The resulting higher modeled discharge has to  
12 be reduced by an increased AET in STANDARD (and in the other model variants) on the land  
13 around the lakes as compared to STRUCTURE (red areas around Great Lakes in Fig. 3).

14 Differences between NoCal and STANDARD are caused by the calibration parameter  $\gamma$   
15 which differs from 1.0 (NoCal) in most cases in STANDARD (and the other model variants).  
16 For example, there are blue patterns in China and South America. In both regions,  $\gamma$  is lower  
17 than 1.0 in STANDARD which results in higher runoff and less modeled AET. In many other  
18 regions (red areas),  $\gamma$  is greater than 1.0 in STANDARD.

19 AET differences between LANDCOVER and STANDARD (Fig. 3c) are caused by changes  
20 in net radiation in energy-limited areas (not shown) as well as changes in rooting depth. In  
21 general, minor differences occur (except in some basins, see explanation below). In some  
22 regions, an increasing net radiation results in an increasing AET, e.g. in parts of Angola. In  
23 water-limited areas (e.g. north eastern Brazil), insignificant changes of AET occur even if net  
24 radiation strongly increases. In northern Australia, AET increases even when net radiation is  
25 reduced. Here, large parts are defined in STANDARD as open shrubland (rooting depth of 0.5  
26 m) and in LANDCOVER as savanna (rooting depth of 1.5 m). As soil storage capacity is a  
27 function of rooting depth, even with more energy available for evapotranspiration, only half  
28 of the soil water can be evapotranspired due to the limited rooting depth. Neglecting human  
29 water abstraction in variant NoUse would lead to an overestimation of AET in regions where  
30 water abstraction for irrigation leads to reduction of wetlands areas (Fig. 3e), and a global  
31 AET overestimation by less than 0.2% (Table 2).

1 In WaterGAP 2.2, AET can become negative in some (mostly snow dominated) regions,  
2 where precipitation input is too low to reproduce observed discharge (grey colors in Fig. 3a).  
3 The total water balance of each large water body is calculated in the outflow cell, hence AET  
4 can become very large as the value in mm is calculated by dividing AET over the whole lake  
5 by grid cell area.

### 6 **3.3 Renewable water resources**

7 RWR (mean annual runoff of the grid cell to the river without consideration of human water  
8 use) are dominantly influenced by the calibration (NoCal) and subsequently by input data and  
9 model structure (Fig. 4).

10 As RWR are approximately the difference between precipitation and AET, the difference  
11 maps (Fig. 4b-e) represent more or less the inverted difference maps of Fig. 3 of the previous  
12 section. Compared to STANDARD, largest differences occur in model variant NoCal. In  
13 contrast to AET, calibration leads in many cases to lower RWR. The global sum of RWR of  
14 NoCal is 15.8% higher than with STANDARD (Table 2). The global sum of RWR from  
15 CLIMATE is 4.7% higher but with large spatial spread. RWR decreases in CLIMATE on  
16 21.4% of land surface by more than  $10 \text{ mm yr}^{-1}$  and increase by more than  $10 \text{ mm yr}^{-1}$  on  
17 29.9% of the land surface. RWR decreases (increases) by more than  $100 \text{ mm yr}^{-1}$  on 4.7%  
18 (9.0%) of the land surface. The differences in LANDCOVER mainly follow differences in net  
19 radiation (not shown). In snow-dominated regions, RWR are lower in STRUCTURE because  
20 snow cover dynamics are less intense than in STANDARD. In grid cells with (large) surface  
21 water bodies, RWR are lower in STRUCTURE (as AET is unlimited here even if storages are  
22 nearly empty).

### 23 **3.4 River discharge**

#### 24 **3.4.1 River discharge seasonality**

25 River discharge is the integral result of runoff generation, water losses by evaporation from  
26 surface water bodies, positive or negative net abstractions from surface water bodies and  
27 groundwater, and routing processes. It is one of the most important diagnostic variables in  
28 water resources. In many regions, river discharges have been observed for decades, providing  
29 an important data source for model evaluation. A good representation of modeled seasonality  
30 in comparison to the observed one is therefore a criterion for model evaluation. We compared

1 observed and modeled discharge seasonality at the outflow of 12 large river basins, covering  
2 different climatic zones and levels of anthropogenic influence (Fig. 5). Climate input and  
3 model structure influence modeled discharge seasonality more than land cover changes for the  
4 selected river basins. Where seasonality of climate is high, like in the monsoon-dominated  
5 Mekong basin, only marginal differences occur due to land cover and model structure.  
6 Structural model refinements have also important effects on discharge seasonality. For  
7 example, the constant flow velocity of STRUCTURE (in contrast to variable flow velocity in  
8 the other variants) leads to a higher peak in the Lena. Here, the variable flow velocity  
9 algorithm underestimates flow velocity in the lower reaches where bed slopes are very small.  
10 This leads to a strong underestimation of peak flow (which explains the improved seasonality  
11 of STRUCTURE compared to observed discharge in the Lena). The reservoir algorithm  
12 which is not enabled in STRUCTURE has impacts at the Yangtze, Rio Parana, Mississippi  
13 and the Volga in terms of smoothing the discharge. For the Rio Parana, this is the main  
14 influence in the STRUCTURE variant. The representation of snow in STANDARD leads to a  
15 more heterogeneous snow coverage as compared to the STRUCTURE variant. The strongest  
16 impact occurs for the Rhine, where the snow algorithm is the dominant reason for the  
17 differences to STRUCTURE. In STRUCTURE, the snow water storage of the Rhine  
18 headwater (Alps) is generally lower. In particular between May and October (the Alps are  
19 modeled as snow-free between June and September), this leads to a decrease of discharge as  
20 snowmelt cannot contribute any longer as it does e.g. in STANDARD. The importance of the  
21 climate forcing can be seen in the Mississippi and the Rhine where CLIMATE results in  
22 overestimated peak seasonal discharge. In the Danube, WFD/WFDEI climate input (in  
23 STANDARD) is particularly beneficial, as the fit to observed seasonality is much better than  
24 with CRU TS 3.2 / GPCC v6 climate (in CLIMATE).

25 For the Mackenzie River, all model variants are close to each other but far away from  
26 observations. Here, freezing and thawing of the river are not reproduced as none of the model  
27 variants represents these processes. Interestingly, the Lena river basin is also frozen during  
28 winter time but here, low flows are simulated quite well. In the Amazon, the model variants  
29 underestimate the delay of peak discharge which might be explained by the lack of modeling  
30 dynamic floodplain inundation.

31 The impact of alternative land cover is only slightly influencing discharge seasonality. Most  
32 effects occur at the Rhine, where CORINE-based land cover (variant LANDCOVER) consists



1 dominantly of cropland. Many grid cells in the other model variants consists of mixed forest  
 2 or cropland / natural vegetation mosaic which both have a lower albedo, resulting in more  
 3 evaporation and less discharge especial in the summer months. Additional effects occur due to  
 4 deeper roots at mixed forest class. Only for the Mackenzie, Lena and Yangtze, mean monthly  
 5 river discharges of NoCal are within the range of all other variants in some months. The  
 6 NoCal values for the Orange River are higher than any observed value (and the values of the  
 7 other variants) throughout the year (Fig. 5). This highlights the need for a calibrated model for  
 8 discharge analyses.

### 9 3.4.2 Monthly time series

10 Nash-Sutcliffe efficiencies  $E_{NS}$  (Eq. 1, Nash and Sutcliffe, 1970) were calculated for time  
 11 series of monthly river discharges at the gauging stations used for calibration.

$$12 \quad E_{NS} = 1.0 - \frac{\sum_{i=1}^n (O_i - S_i)^2}{\sum_{i=1}^n (O_i - \bar{O})^2} \quad (1)$$

13 with  $O_i$  is observed discharge,  $S_i$  is simulated discharge and  $\bar{O}$  is mean observed discharge  
 14 (all units in  $\text{km}^3 \text{ month}^{-1}$ ).

15 By adjusting the mean annual river discharge as done in our calibration approach,  $E_{NS}$  of  
 16 monthly discharge increases in all calibrated model variants as compared to the NoCal  
 17 variant, because  $E_{NS}$  is sensitive to both mean and variances (Fig. 6). Among all calibrated  
 18 variants, STANDARD and NoUse achieve the highest mean  $E_{NS}$  values, while variant  
 19 STRUCTURE shows a distinctly lower model performance (Fig. 6). This is further confirmed  
 20 by the  $E_{NS}$  distribution per Köppen-Geiger region (Table 4, column “sum”), where in case of  
 21 STANDARD and NoUse,  $E_{NS}$  is larger than 0.5 in 53.5% of the basins. Comparing  
 22 STANDARD and STRUCTURE, model development clearly improved simulation results in  
 23 A, C and D climates. The CLIMATE variant performs better in cold areas but overall  
 24 performs worse than STANDARD, in particular in temperate climate. No significant  
 25 differences occur when using an alternative land cover input (LANDCOVER). Performance  
 26 of all variants is very poor in arid (B) climate.

### 1 **3.5 Variations of total water storages**

2 Simulated temporal variations of TWS, i.e. the total amount of water in all continental water  
3 storage compartments (Fig. A1), are used widely in the context of analyzing information  
4 derived from the Gravity Recovery and Climate Experiment (GRACE). The dominant  
5 seasonal changes of TWS can be characterized by the difference between the minimum and  
6 the maximum value of mean monthly TWS (1971-2000). The spatial distribution of seasonal  
7 TWS variations (Fig. 7a) is similar to that derived with an earlier version of WaterGAP (see  
8 Fig. 4 in Güntner et al. (2007)). Seasonal TWS variations are affected most strongly by the  
9 climate forcing (Fig. 7b). For example, in Europe and eastern US, they are more than 25 mm  
10 higher in case of CRU/GPCC climate forcing. This finding is consistent with the impact of  
11 climate forcing on river discharge, e.g. of the Danube (Fig. 5). The calibration approach leads  
12 to a decrease of TWS variation in areas where runoff is overestimated (Fig. 7f). Where land  
13 cover attributes vary significantly due to different land cover classes in LANDCOVER,  
14 effects on TWS variations are strong (e.g. in Southern Congo or in Southern Amazon).  
15 Neglecting groundwater abstractions (as done in NoUse, which neglects any human water  
16 use, and in STRUCTURE, where water is only abstracted from surface waters) leads to lower  
17 seasonal TWS variations in areas of groundwater abstractions (if in case of STRUCTURE,  
18 surface water is not able to satisfy water uses) and groundwater depletion (e.g. High Plains  
19 Aquifer in central USA, Iran and Northwestern India) (Fig. 7d and e). In these two variants,  
20 seasonal groundwater storage variations are solely driven by seasonal variations of  
21 groundwater recharge. Without simulating water use, some areas with large surface water  
22 irrigation have higher seasonal variations than with water use because large return flows  
23 during the dry (irrigation) season smooth natural groundwater storage variations.

24 In addition, seasonal TWS variations in STRUCTURE differ from STANDARD particularly  
25 along large rivers (Fig. 7d), mostly with a smaller range in STRUCTURE. There, the flow  
26 velocity (variable in STANDARD) is lower than the constant  $1 \text{ m s}^{-1}$  in STRUCTURE,  
27 resulting in increased river storage. In many cold areas, the simpler snow algorithm in  
28 STRUCTURE leads to increased TWS seasonality.

## 1 **4 Discussion**

### 2 **4.1 Comparison of simulated freshwater fluxes to other estimates**

3 The modeled AET and discharge to the oceans and inland sinks for all model variants are  
4 within the range of published values except the NoCal variant, which has very low AET and  
5 high discharge values (Tables 2 and 5). Discharge estimates differ due to the applied  
6 estimation method and precipitation data set. Mueller et al. (2013) do not consider  
7 precipitation undercatch correction and assume a global precipitation of  $\sim 99\,000\text{ km}^3\text{ yr}^{-1}$   
8 which is low compared to recent estimates of Schneider et al. (2014) ( $117\,000\text{ km}^3\text{ yr}^{-1}$ ) or the  
9 values used in this study (Table 2). Compared to previous WaterGAP results, model  
10 refinements have led to an increase of discharge. The value of STANDARD is approx.  $450$   
11  $\text{km}^3\text{ yr}^{-1}$  higher than for STRUCTURE (Table 2), and previous estimates (Döll et al., 2003)  
12 are even lower as precipitation undercatch was not taken into account.

### 13 **4.2 Advantages and limitations of the calibration approach**

14 The applied calibration approach is clearly beneficial as it leads to a better fit of simulated to  
15 observed monthly river discharge time series (Fig. 6 and Table 4). Consequently, the basin-  
16 specific adjustment of 1-3 parameters ( $\gamma$ , CFA and CFS, see Appendix B1) based on  
17 observed mean annual discharge has been a part of the WaterGAP modeling approach since  
18 the beginning. Calibration allows to a certain degree compensating errors in input data and  
19 effective model parameters. Also, structural problems of the model, e.g. due to the simplified  
20 representation of hydrological processes at a half-degree grid cell, may be balanced out. The  
21 effect of calibration on modeled renewable water resources (Fig. 4e) dominates all other  
22 modifications within this experiment setup.

23 However, the correction of total cell runoff using CFA and CFS that is required to force  
24 simulated mean annual river discharge values to be equal to observed values is not ideal and  
25 has undesirable effects on estimated AET and RWR. In the Yenisey basin upstream Igarka  
26 (western Siberian Plain), AET is largely reduced in one half of the basin (and vice versa)  
27 when using alternative climate forcing. Transferring the correction factor CFS (which is, if  
28 necessary, calculated at the outflow grid cell of the basin) to the upstream grid cells can lead  
29 to unrealistic high positive and negative values for AET if precipitation is too low in these  
30 parts of the basin to simulate observed discharge or the AET of surface water bodies has to be

1 reduced by CFA. This is the reason for some artificial patterns in Fig. 3 and consequently in  
2 Fig. 4. These kinds of consistency errors can be found in some more basins where cumulative  
3 AET is low and parts of the basins are covered with surface water bodies. Nevertheless, the  
4 approach ensures a closed water balance for the whole basin.

5 Obviously, one parameter is not sufficient to calibrate the model. In many basins the  $\gamma$   
6 parameter is not sensitive to input data and model structure in the current calibration approach  
7 as the range of  $\gamma$  through all four variants (NoCal is not considered, NoUse has the same  
8 value as STANDARD) is rather small. 59% of the basins in Fig. 8 are colored dark blue  
9 which means that the calibration parameter  $\gamma$  has the same value in all model variants. Here,  
10  $\gamma$  is at its artificial minimum (0.1) or maximum (5.0) value, and the influence of input data  
11 and model structure, which were modified in this experiment, is insignificant. On the other  
12 hand, in 21% of the basins,  $\gamma$  is differing by  $> 1$  (green, yellow and red colors). In these  
13 basins, the calibration parameter is sensitive to input data and model structure. Anyhow,  
14 within future model development, one task is to restructure the calibration approach with the  
15 aim to avoid correction factors or rather to introduce and test alternative calibration  
16 objectives. This could be achieved by either including more parameters (multi-parameter  
17 calibration) and/or by integrating additional reference data, e.g. GRACE based data as was  
18 shown by Werth and Güntner (2010) (multi-objective calibration). In addition, remote sensing  
19 based input data with global coverage have been available for a decade. Especially for land  
20 cover characteristics (e.g. land cover type,  $L$ , albedo, see Appendix A), a more realistic  
21 representation of dynamics (integration of time series as input data instead of static input  
22 maps) can reduce the input data and model parameter uncertainty.

#### 23 **4.3 How sensitive are freshwater fluxes and water storages to spatially** 24 **distributed input data (climate forcing, land cover)?**

25 In general, more differences occur due to the alternative climate input than due to the  
26 alternative land cover data. The major freshwater fluxes (AET, Fig. 3 and RWR, Fig. 4) as  
27 well as river discharge (Fig. 5) show in many cases that land cover input has much less impact  
28 (except for some areas where the attributes of a changed land cover type differ significantly).  
29 The effect of different land cover input would probably increase if the associated attributes  
30 were also modified. Forced with CRU 3.2 and GPCC v6 instead of WFD/WFDEI input, AET  
31 is increased by at least  $10 \text{ mm yr}^{-1}$  in large parts in the world (light blue colors in Fig. 3b). In

1 those regions with similar precipitation amounts but different radiation, RWR decreases by  
2 the same amount as AET increased (e.g. South East Asia, Australia, Saudi Arabia). In other  
3 regions, no clear effect on RWR is detectable (e.g. North America). In some parts of Europe,  
4 RWR increases by at least  $10 \text{ mm yr}^{-1}$  even if AET increases. Here, besides radiation  
5 (affecting AET), the amount of precipitation is of great importance (affecting RWR).

6 In regions where the climate forcing datasets differ significantly (e.g. Danube River Basin),  
7 the impact on discharge is large (Fig. 5 bottom center). Here, differences in temperature and  
8 precipitation amounts lead to a poor fit compared to observed discharge when using the  
9 CLIMATE variant which is also reflected in the  $E_{NS}$  criterion (Fig. 9b). Also, the two land  
10 cover input data sets used here result in the same  $E_{NS}$  classes, with only a few exceptions  
11 (Fig. 9c).

#### 12 **4.4 What are the benefits of WaterGAP model structure refinements** 13 **implemented during the last decade?**

14 In general, WaterGAP 2.2 STANDARD leads to improved results compared to the reduced  
15 model version STRUCTURE that is comparable to the Döll et al. (2003) model version. In  
16 many basins in the alpine region in central Europe,  $E_{NS}$  of STRUCTURE ranks behind  
17 STANDARD (Fig. 9d, red colors) reflecting a refined simulation of snow cover dynamics on  
18 the 3 arc minute sub-grid. In some basins, the reservoir algorithm improves  $E_{NS}$  (and  
19 discharge seasonality). For example, the Volga at station Volgograd Power Plant (see also  
20 Fig. 5) and basins in Brazil show a much better  $E_{NS}$  (Fig. 9d) in STANDARD compared to  
21 STRUCTURE. However,  $E_{NS}$  of some basins with  $E_{NS} < 0.5$  in STANDARD is improved in  
22 STRUCTURE. In summary, integrating more complex and refined process descriptions (see  
23 Sect. 2.2.3) in the past decade has led to improved simulation of monthly time series of river  
24 discharge with WaterGAP. However, discharge before calibration tends to be higher with the  
25 implemented structural changes, e.g. due to the storage-dependent reduction of surface water  
26 evaporation. This together with the use of more calibration stations (Hunger and Döll, 2008)  
27 and the introduction of a bias-correction for observed precipitation (Döll and Fiedler, 2008)  
28 has had the problematic consequence that correction factors to lower simulated river  
29 discharge have increasingly been required to ensure that simulated mean annual river  
30 discharges are equal to observed values.

#### 1 **4.5 How does the modeling approach (calibration procedure, consideration of** 2 **human water use) affect freshwater fluxes and water storages?**

3 The calibration procedure reduces simulated river discharge and water resources on most of  
4 the land area and increases the AET (Figs. 3 and 4, Table 2). Without calibration, global AET  
5 and discharge would rank at the lower and higher end of the published values, respectively  
6 (Table 5). In addition, the fit to observed monthly river discharge time series as quantified  
7 using the  $E_{NS}$  criterion would worsen almost everywhere (Fig. 9f). The impact of calibration  
8 on freshwater fluxes and water storages is higher than those of alternative climate forcings  
9 and land cover data, and of a more sophisticated model structure. This confirms the strong  
10 benefit of calibration. However, as  $E_{NS}$  is affected by mean discharge as well as discharge  
11 variations, the calibration approach improves this criterion.

12 Compared to the other variants, the consideration of human water use does not have large  
13 effects on freshwater fluxes and storages at the global scale. In regions with intense water use,  
14 in particular from surface water bodies (e.g. in Pakistan), AET without considering additional  
15 evaporation from  $WC_a$  (Table 2) is reduced due to human water use (Fig. 3e). This effect  
16 occurs because human water uses decrease surface water storages and thus the reduction  
17 factor decreases evaporation from surface water bodies (Appendix A5). If the impact of  
18 human water use on river discharge were not considered, van Beek et al. (2011) showed lower  
19 performance in general. Within our experiment, higher correction factors would be necessary  
20 in basins with large abstractions from surface water bodies or significant decreases of  
21 baseflow due to groundwater abstractions. Still,  $E_{NS}$  of basins with high amounts of human  
22 water use is generally lower than those without human water use (not shown). In some basins  
23 mainly in northeastern Europe,  $E_{NS}$  improves when neglecting human water use (Fig. 9e).  
24 This obviously reflects uncertainties in water use models.

#### 25 **4.6 Which type of uncertainty is dominant for specific fluxes and variations of** 26 **total water storage?**

27 The answer to this question depends on the type of fluxes and the spatial aggregation.  
28 Regarding selected global sums of freshwater fluxes (Q and AET) and mean annual total  
29 water storage trends dTWS, dominant uncertainties can be determined by computing  
30 differences between the values computed with a certain model variant and STANDARD. As

1 already shown above, global values of AET and Q as well as the fit of simulated to observed  
2 river discharge time series ( $E_{NS}$ ) are most sensitive to whether the model is calibrated or not  
3 (Table 6). STRUCTURE and NoUse have the strongest impact on the global TWS trend  
4 (Table 6) as these model variants cannot reflect groundwater depletion. More refined model  
5 algorithms rank second regarding global AET sums and  $E_{NS}$ , and alternative climate forcings  
6 rank second regarding river discharge and third regarding median  $E_{NS}$ . The alternative land  
7 cover input data sets have the overall lowest impact on computed freshwater fluxes and  
8 storages.

9 Regarding grid cell-specific differences that are more relevant than global values for most  
10 applications, the ranking of dominant uncertainties is quite different. Patterns of seasonal  
11 TWS variations are affected most strongly by the climate forcing (Fig. 7b), while climate  
12 forcings show the second largest impact on the spatial distribution of AET and RWR, after  
13 calibration (Figs. 3 and 4). The fraction of the global land area that is affected by significant  
14 differences of AET and river discharge between a certain model variant and the STANDARD  
15 variant is largest in case of NoCal, followed by CLIMATE, LANDCOVER, STRUCTURE  
16 and NoUse. Thus, both global and grid cell values are most sensitive to calibration. The larger  
17 sensitivities to climate forcings and land cover input at the grid cell level (Table 7) cancel  
18 when globally averaged. The larger sensitivities of globally aggregated values (Table 6) to  
19 structural changes and the consideration of water use is due to unidirectional changes for all  
20 affected grid cells, but different to alternative climate and land cover data, structural changes  
21 and water use only affect a limited number of grid cells. This discussion on the dominant type  
22 of uncertainty does not take into account parameter uncertainty which is a major additional  
23 source of uncertainty (Kaspar, 2003).

## 24 **5 Conclusions**

25 We studied the sensitivity of freshwater fluxes and storages as computed by the GHM  
26 WaterGAP 2.2 to spatially distributed input data (climate forcing and land cover input) as  
27 well as model structure (model refinements during the last decade), consideration of human  
28 water use and calibration (or no calibration). We designed five model variants in addition to  
29 the standard variant. In each model variant, one component or feature was modified with  
30 respect to the standard variant. Sensitivity of different freshwater fluxes and water storage  
31 variations to the five types of uncertainty were analyzed and ranked considering both global

1 sums and grid cell values, taking into account also the capability of the model variants to  
2 simulate time series of observed river discharge. Basin-specific calibration to mean annual  
3 river discharge was found to have the strongest impact on fluxes and storage variation and is  
4 the dominant reason for an improved simulation of observed monthly river discharge time  
5 series (as characterized by the Nash-Sutcliffe criterion). Uncertainty due to alternative climate  
6 forcing, and to a lesser extent, land cover input, leads to significant variations of grid cell  
7 fluxes (actual evapotranspiration, renewable water resources and river discharge) and storages  
8 (seasonal range of total water storage) even if the model variants are individually calibrated.  
9 However, these uncertainties largely cancel at the global scale while the more refined model  
10 structure, and to a lesser extent water use, are more important for global sums of river  
11 discharge and actual evapotranspiration but also for an improved fit to observed monthly time  
12 series of river discharge.

13 The STANDARD variant of WaterGAP 2.2 leads to the best fit to observed river discharge  
14 (monthly time series, Fig. 6 and Table 4, and seasonality, Fig. 5). We conclude that the daily  
15 WFD/WFDEI data set as climate forcing is preferable to using a combination of the monthly  
16 CRU 3.2 and GPCC v6 data sets as done for model variant CLIMATE. However, we found  
17 that it is problematic to combine the WFD climate data set (covering 1901-2001) with the  
18 only seemingly consistent WFDEI data set (covering 1979-2009) due to a radiation bias (short  
19 wave downward radiation component) between the two data sets. This results in a steep  
20 increase of actual evapotranspiration in 1979, and a water storage decrease between 1971 and  
21 2000 that is an artifact of the combination of the two climate data sets (comp. Sect. 3.1). It  
22 would be very beneficial for an improved estimation of global freshwater fluxes and storages  
23 to have a consistent daily climate forcing that covers the whole 20<sup>th</sup> and the early 21<sup>st</sup> century.

24 The calibration approach of WaterGAP is necessary to compensate uncertainties of spatially  
25 distributed input data, parameters and model structure. However, a calibration of only one  
26 parameter related to soil water balance is not sufficient and correction factors have to be  
27 applied in a number of basins. Therefore, a redesign of the calibration approach, with  
28 additional observations (e.g. including TWS variations as derived from GRACE gravity  
29 fields), other calibration objectives and adjustment of more model parameters (without  
30 correction factors) is planned.

31 The improved representation of hydrological processes of WaterGAP within the last decade  
32 led to a more complex model structure. In most cases, those modifications resulted in a better



1 fit to observed river discharge. However, in some parts of the world, model performance is  
2 still not satisfactory due to an inappropriate modeling of certain processes such that further  
3 changes of the model structure are required. For example, the modeled discharge seasonality  
4 in the Amazon basin is shifted compared to the observed one, which is suspected to be caused  
5 by inappropriate modeling of the temporal variations of inundations and the neglect of  
6 backwater effects. The reservoir operation algorithm does not yet take into account the  
7 construction year of the dam. Moreover, model results in semi-arid and arid regions are poor,  
8 and improved modeling of evaporation from ephemeral ponds is planned.

9

10

## 1 **Appendix**

2 Appendix A describes the WaterGAP Global Hydrology Model (WGHM) in its current  
3 version 2.2. In the order of processing, the single storage compartments and belonging in- and  
4 outflows are explained. Appendix B provides information on the calibration and  
5 regionalization approach WaterGAP is based on. Appendix C gives a brief introduction of the  
6 water use sub-models, and the GWSWUSE module is described in Appendix D.

### 7 **Appendix A: Description of the WaterGAP Global Hydrology Model (WGHM)**

#### 8 **A1 Canopy**

9 The change of canopy storage  $S_c$  [mm] over time  $t$  [ $^{-1}$ ] is calculated as

$$10 \quad \frac{dS_c}{dt} = P - P_t - E_c \quad (\text{A1})$$

11 where precipitation  $P$  [mm d $^{-1}$ ] is the inflow and the amount of throughfall  $P_t$  [mm d $^{-1}$ ] and  
12 canopy evaporation  $E_c$  [mm d $^{-1}$ ] are the outflows.

13 Throughfall  $P_t$  is calculated as

$$14 \quad P_t = \begin{cases} P & S_c \geq S_{c,\max} \\ 0 & S_c < S_{c,\max} \end{cases} \quad (\text{A2})$$

15 Following Deardorff (1978), canopy evaporation  $E_c$  is calculated as

$$16 \quad E_c = E_p \left( \frac{S_c}{S_{c,\max}} \right)^{\frac{2}{3}} \quad (\text{A3})$$

17 where  $E_p$  is potential evapotranspiration [mm d $^{-1}$ ].

18  $E_p$  is calculated according to the Priestley-Taylor model (Priestley and Taylor, 1972),  
19 differentiating atmospheric water demand between humid ( $\alpha = 1.26$ ) and semi-arid / arid ( $\alpha =$   
20 1.74) areas. Grid cells were defined as semi-arid / arid if long term average (1971-2000)  
21 precipitation is less than  $0.5 \times E_p$  (UNEP, 1992).

22  $S_c$  is limited between 0 and maximum canopy storage  $S_{c,\max}$ , which is calculated as

$$1 \quad S_{c,\max} = m_c L \quad (\text{A4})$$

2 where  $m_c$  is 0.3 [mm] and  $L$  is the leaf area index [-].  $L$  is calculated based on a modified  
3 growth model described in Kaspar (2003) and is limited to minimum and maximum values.  
4 Maximum  $L$  values per land cover class (Table A1) are based on literature (Schulze et al.,  
5 1994; Scurlock et al., 2001). Minimum  $L$  values per land cover class are calculated as:

$$6 \quad L_{\min} = 0.1 f_{d,lc} + (1 - f_{d,lc}) c_{e,lc} L_{\max} \quad (\text{A5})$$

7 where  $f_{d,lc}$  is the fraction of deciduous plants [-] and  $c_{e,lc}$  is the reduction factor for evergreen  
8 plants [-] (Table A1). Development of  $L$  is simulated as a function of daily temperature and  
9 precipitation. The growing season starts when the daily temperature is above 8 °C for a land  
10 cover specific number of days (Table A1) and cumulative precipitation is at least 40 mm.  
11 During the growing season,  $L$  increases linearly until it reaches  $L_{\max}$  after 30 days. In semi-  
12 arid and arid regions, it is necessary that at least 0.5 mm daily precipitation occurs to keep the  
13 growing season ongoing. If the condition for growing season is not fulfilled anymore, the  
14 senescence phase is initiated, i.e.  $L$  is degraded to  $L_{\min}$  linear within 30 days.

## 15 **A2 Snow**

16 The change of snow water storage  $S_{sn}$  [mm] over time  $t$  [ $\text{d}^{-1}$ ] is calculated as

$$17 \quad \frac{dS_{sn}}{dt} = P_{sn} - M - E_{sn} \quad (\text{A6})$$

18 where  $P_{sn}$  is precipitation, falling as snow at temperatures below 0 °C [ $\text{mm d}^{-1}$ ],  $M$  is snow  
19 melt [ $\text{mm d}^{-1}$ ] and  $E_{sn}$  is sublimation [ $\text{mm d}^{-1}$ ].

20 Snow accumulation and melt are modeled on a 3 arc minute sub-grid (100 sub-grid cells per  
21 0.5°) using a degree day algorithm (Schulze and Döll, 2004). Mean sub-grid elevation was  
22 derived from GTOPO30 (U.S. Geological Survey, 2003). The daily temperature for each sub-  
23 grid cell is calculated from the temperature of the 0.5° cell, applying an adiabatic lapse rate of  
24 0.6 °C per 100 m. To avoid excessive snow accumulation, temperature does not decrease if a  
25 snow water equivalent of 1000 mm is reached in one sub-grid.

26 At temperatures below 0 °C, all precipitation is assumed to fall and accumulate as snow. At  
27 sub-grid temperatures  $T$  [°C] above melting temperature  $T_m$  (0 °C) and if snow storage is

1 present, snow melts with land cover specific degree-day factor  $D_F$  [ $\text{mm d}^{-1} \text{ } ^\circ\text{C}^{-1}$ ] (Table A2)  
 2 as:

$$3 \quad M = \begin{cases} D_F(T - T_m) & T > T_m, \quad S_{sn} > 0 \\ 0 & \text{other} \end{cases} \quad (\text{A7})$$

4 Instead of using one specific albedo for snow as in previous versions ( $\alpha = 0.4$ ), land cover  
 5 specific snow albedo values are used to account for differences in reflective properties  
 6 between the land use classes under snow-covered conditions (Table A2). The albedo value  
 7 switches to snow albedo if snow water equivalent of the grid cell exceeds 3 mm, i.e. a closed  
 8 snow cover is assumed. Sublimation  $E_{sn}$  is modeled like potential evaporation rate but  
 9 applying a latent heat of 2.835 [ $\text{MJ kg}^{-1}$ ] for temperatures below 0  $^\circ\text{C}$  and  $2.501 - 0.002361 \times$   
 10  $T$  [ $\text{MJ kg}^{-1}$ ] above 0  $^\circ\text{C}$ .

### 11 **A3 Soil**

12 Like snow and canopy, the change of soil water storage  $S_s$  [mm] over time  $t$  [ $^{-1}$ ] is calculated  
 13 as one layer as:

$$14 \quad \frac{dS_s}{dt} = P_{eff} - R_l - E_s \quad (\text{A8})$$

15 with effective precipitation  $P_{eff}$  [ $\text{mm d}^{-1}$ ] as inflow and runoff from land  $R_l$  [ $\text{mm d}^{-1}$ ] and  
 16 actual evapotranspiration  $E_s$  [ $\text{mm d}^{-1}$ ] as outflows.

$$17 \quad P_{eff} = P_t - P_{sn} + M \quad (\text{A9})$$

18 with  $P_t$  is through fall [ $\text{mm d}^{-1}$ ], (see Sect A1),  $P_{sn}$  is precipitation falling as snow [ $\text{mm d}^{-1}$ ]  
 19 and  $M$  is snow melt [ $\text{mm d}^{-1}$ ].

20 Actual evapotranspiration from the soil  $E_s$  [ $\text{mm d}^{-1}$ ] is a function of potential  
 21 evapotranspiration from the soil  $E_p$  [ $\text{mm d}^{-1}$ ] minus the already evaporated water from the  
 22 canopy  $E_c$  [ $\text{mm d}^{-1}$ ], actual soil water content in the effective root zone  $S_s$  [mm] and total  
 23 available soil water capacity  $S_{s,max}$  [mm] as

$$24 \quad E_s = \min\left( (E_p - E_c), (E_{p,max} - E_c) \frac{S_s}{S_{s,max}} \right) \quad (\text{A10})$$

1 where  $E_{p,\max}$  is 20 mm d<sup>-1</sup> in semi-arid and arid regions whereas 10 mm d<sup>-1</sup> in grid cells  
 2 classified as humid,  $S_{s,\max}$  is the product of total available water capacity in the upper meter  
 3 of the soil (Batjes, 1996) and the land cover specific rooting depth (Table A2).

4 Runoff from land  $R_l$  [mm d<sup>-1</sup>] is calculated after Bergström (1995) as

$$5 \quad R_l = P_{eff} \left( \frac{S_s}{S_{s,\max}} \right)^\gamma \quad (A11)$$

6 Dependent on the soil water storage  $S_s$ , a part of effective precipitation  $P_{eff}$  becomes runoff.  
 7 If the soil water storage is empty,  $R_l = 0$ . If the soil is completely saturated (at  $S_{s,\max}$ ), runoff  
 8 equals effective precipitation. Between these points, the runoff coefficient  $\gamma$  determines the  
 9 amount of precipitation that converts to runoff. This parameter is used for calibration (see  
 10 Sect. B1). In urban areas (defined as separate input map from IMAGE 2.2), 50% of  $P_{eff}$  is  
 11 directly passed to the river.

## 12 **A4 Groundwater**

13 Inflow to groundwater storage  $S_g$  [mm] is groundwater recharge  $R_g$  [mm d<sup>-1</sup>], whereas  
 14 outflows are baseflow  $Q_g$  [mm d<sup>-1</sup>] and net abstractions from groundwater  $NA_g$  [mm d<sup>-1</sup>]  
 15 (Section C), which can also act as inflow (e.g. as additional groundwater recharge due to  
 16 irrigation with surface water).

$$17 \quad \frac{dS_g}{dt} = R_g - Q_g - NA_g \quad (A12)$$

18 Groundwater recharge  $R_g$  [mm d<sup>-1</sup>] is calculated as a fraction of runoff from land:

$$19 \quad R_g = \min(R_{g,\max}, f_g R_l)$$

20 where  $R_{g,\max}$  is soil texture specific maximum groundwater recharge [mm d<sup>-1</sup>] (with values of  
 21 7/4.5/2.5 for sandy/loamy/clayey soils) and  $f_g$  is the groundwater recharge factor (ranging  
 22 between 0 and 1) related to relief, soil texture, aquifer type and the existence of permafrost or  
 23 glaciers. For a detailed description see Döll and Fiedler (2008). If a grid cell is defined as arid  
 24 and has coarse (sandy) soil, groundwater recharge will only occur if precipitation exceeds a

1 critical value of  $12.5 \text{ mm d}^{-1}$ . Both values,  $R_{g,\max}$  and the precipitation threshold, are adapted  
2 to the climate forcing used (WFD) aiming to reach comparable groundwater recharge patterns  
3 of (Döll and Fiedler, 2008) as that groundwater recharge estimation is confirmed with experts  
4 within the WHYMAP (<http://www.whymap.org>) efforts. Within CLIMATE, the original  
5 values 5/3/1.5 for  $R_{g,\max}$  and  $10 \text{ mm d}^{-1}$  as precipitation threshold were used.

6 The outflow is modeled with  $k_g = 0.01 \text{ d}^{-1}$  as

$$7 \quad Q_g = k_g S_g \quad (\text{A13})$$

8 The runoff from land  $R_l$ , which is not groundwater recharge  $R_g$ , represents the fast surface  
9 runoff  $R_s$  and is routed, together with  $Q_g$ , through a series of different storages representing  
10 wetlands, lakes and reservoirs until reaching the river segment (Fig. A1).

## 11 **A5 Surface water bodies**

12 Surface water bodies (inland freshwater such as wetlands, lakes and reservoirs) play an  
13 important role in the hydrologic cycle e.g. for evaporation and the lateral transport. In general,  
14 surface water body storages  $S$  [ $\text{m}^3$ ] increase by inflow  $I$  [ $\text{m}^3 \text{ d}^{-1}$ ] from other storages or from  
15 upstream (see Fig. A1), and are reduced by the outflow  $Q$  [ $\text{m}^3 \text{ d}^{-1}$ ]. Additionally, the water  
16 balance of the water body itself  $B$  [ $\text{m}^3 \text{ d}^{-1}$ ] is calculated as  $B = P - E_w$ , where  $P$  is  
17 precipitation [ $\text{m}^3 \text{ d}^{-1}$ ] and  $E_w$  is potential evaporation of open water surfaces [ $\text{m}^3 \text{ d}^{-1}$ ] applying  
18 an albedo of 0.08. Finally, net abstractions of surface water  $\text{NA}_s$  [ $\text{m}^3 \text{ d}^{-1}$ ] are considered,  
19 resulting in the storage equation:

$$20 \quad \frac{dS}{dt} = I - Q + B - \text{NA}_s \quad (\text{A14})$$

21 Outflow is in principle modeled like groundwater outflow (Sect. A4) for “local” lakes and  
22 wetlands, whereas “global” lakes and wetlands are linear storages whose equations are solved  
23 analytically.

24 WaterGAP 2.2 does not consider variable land/water fractions as would be expected when a  
25 lake is shrinking due to evaporation and land surface increases; thus Hunger and Döll (2008)  
26 introduced a reduction parameter which reduces the evaporation when lake / wetland storage  
27 is low. In WaterGAP 2.2, for all surface water bodies the reduction factor  $r$  [-] is calculated as

$$r = 1 - \left( \frac{|S - S_{\max}|}{S_{\max}} \right)^p \quad (\text{A15})$$

where  $S$  is actual water body storage [ $\text{m}^3$ ],  $S_{\max}$  is maximum water body storage [ $\text{m}^3$ ] and  $p$  is the reduction exponent [-]. As no truly global dataset on lake volumes is available, the maximum storage capacity is determined by multiplying the surface area with an “active” depth (set to 5 m and 2 m for lakes and wetlands, respectively). Values for  $p$  are 3.32 for lakes and wetlands which means a reduction of evaporation by 10% if storage is halved and 2.81 for reservoirs, which means a reduction of 15% if storage is half of the maximum storage capacity (and a reduction of 50% if storage is reduced to 20% of storage capacity).

The distribution of wetlands is derived from GLWD (Lehner and Döll, 2004) as percentage of cell coverage. Locations and attributes of lakes and reservoirs are based on a combination of GLWD and a preliminary version of the GRanD database (Döll et al., 2009; Lehner et al., 2011). In total, 6553 reservoirs, 52 regulated lakes (lakes whose outflow is regulated by a dam) (from GRanD) and 242 798 unregulated lakes (from GLWD) were considered. Out of these, 1386 large lakes (area  $\geq 100 \text{ km}^2$ ), 1110 large reservoirs (storage capacity  $\geq 0.5 \text{ km}^3$ ) and 52 regulated lakes (area  $\geq 100 \text{ km}^2$  or storage capacity  $\geq 0.5 \text{ km}^3$ ) were classified as “global”, i.e. they receive inflow not only from the grid cell itself but also from upstream (“global” wetlands are defined in the same way, see Fig. A1). All other surface water bodies were classified as “local”. If “global” lakes or reservoirs cover more than one grid cell, the water balance of the whole surface water body is calculated at the outflow cell.

## 20 **A6 Lateral routing**

The global drainage direction map DDM30 (Döll and Lehner, 2002) is used to route the discharge through the stream network until it reaches the ocean or an inland sink. Fast runoff  $R_s = R_t - R_g$  is routed to the surface storages without any delay, whereas baseflow  $Q_g$  is a function of groundwater storage (Fig. A1, Appendix A4). Due to limited information on groundwater flow between grid cells, the groundwater recharge can only contribute to groundwater runoff of the same grid cell.

Verzano et al. (2012) improved the routing by introducing a variable flow velocity approach based on the Manning-Strickler equation. The roughness coefficient is calculated after Cowan (1956) by using different physiographic parameters and information about rural and urban

1 areas. The hydraulic radius is calculated using actual discharge of the cell and empirical  
2 relationships of river width and depth at bankfull flow conditions. Bankfull conditions are  
3 assumed to correspond to the 1.5 year maximum series annual flow (Schneider et al., 2011)  
4 and were accordingly calculated from daily discharge time series for the global land surface.  
5 River bed slopes were calculated based on the HydroSHEDS drainage direction map (Lehner  
6 et al., 2008) and a meandering ratio (method is described in Verzano et al. (2012)).

7 The reservoir algorithm of Hanasaki et al. (2006), distinguishing irrigation and non-irrigation  
8 reservoirs and considering 1109 reservoirs was implemented and improved by Döll et al.  
9 (2009) and slightly adapted in WaterGAP 2.2: If reservoir storage falls below 10% of storage  
10 capacity, the release coefficient is set to 0.1 instead of 0.0 in Döll et al. (2009), assuring that  
11 at least some water is released e.g. for downstream ecosystem demands.

## 12 **Appendix B: Calibration and regionalization**

### 13 **B1 Calibration approach**

14 WGHM is calibrated against mean annual discharge by adjusting the runoff coefficient  $\gamma$   
15 (Eq. A11) for all grid cells of each calibration basin and – if necessary – two additional  
16 correction factors. The calibration procedure of WGHM is described in Döll et al. (2003) and  
17 Hunger and Döll (2008). As WaterGAP was developed to quantify water resources and water  
18 stress, calibration forces simulated discharge to be, during the calibration period, between 99  
19 and 101% of observed river discharge. It is implicitly assumed that the model should be  
20 robust enough to reproduce intra- and interannual variability. Main reasons for calibration are  
21 the uncertainty of input data, parameters and model structure as well as the scale of the model  
22 and grid cell heterogeneity. To overcome overparameterization and to keep the calibration as  
23 simple as possible, calibration is performed by adjusting the one free parameter  $\gamma$  (Eq. A11)  
24 within the limits 0.1 and 5.0. With low  $\gamma$ , runoff is high even if the soil is at low saturation,  
25 and with a high value, runoff is small even with nearly saturated soils. However, in many  
26 basins, adjustment of the soil water balance alone does not lead to a fit of simulated discharge  
27 to observed discharge for various reasons. These include uncertainty of climate forcing,  
28 underestimation of evaporation losses in dry areas caused by neglecting formation of  
29 ephemeral ponds and neglecting of streambed losses. In these cases, the area correction factor  
30 (CFA) is computed, which adjusts net cell runoff of each cell in the sub-basins. With limits



1 between 0.5 and 1.5, cells with positive (precipitation > evapotranspiration) and negative  
2 (water body evapotranspiration > precipitation, e.g. global lakes which are fed by upstream  
3 inflow) are multiplied with a value symmetric around 1.0 (Hunger and Döll, 2008). In some  
4 basins, however, the adaptation of both  $\gamma$  and CFA is not sufficient for a successful  
5 calibration, i.e. the deviation between simulated and observed long term average discharge  
6 remains larger than 1%. Possible reasons are discussed in Hunger and Döll (2008). To avoid  
7 error propagation to next the downstream basin, the modeled discharge is corrected to the  
8 measured discharge in the grid cell where the discharge station is located by multiplying with  
9 the station correction factor CFS (Hunger and Döll, 2008).

## 10 **B2 Discharge stations used**

11 Observed discharge time series were provided by the Global Runoff Data Center (GRDC).  
12 Following Hunger and Döll (2008), gauging stations listed in the GRDC catalogue  
13 (<http://grdc.bafg.de/>, download date: 28.09.2012) were included in the calibration setup if  
14 they fulfilled three main criteria: (1) an upstream area of at least 9000 km<sup>2</sup>, (2) a time series of  
15 at least four (complete) years, and (3) an inter-station catchment area of at least 30 000 km<sup>2</sup>.  
16 All in all, a number of 1319 stations, covering 53.6% of the global land area except Antarctica  
17 and Greenland, was used for calibration (Fig. B1). If available, the 30-year period 1971 to  
18 2000 was chosen as calibration years.

## 19 **B3 Regionalization**

20 In order to transfer the calibrated  $\gamma$  values to ungauged basins, the parameter is regionalized  
21 using a multiple linear regression approach relating the natural logarithm of the calibrated  $\gamma$   
22 values to the following basin descriptors: mean annual temperature, mean available soil water  
23 capacity, fraction of open water bodies, mean basin land surface slope, fraction of permanent  
24 snow and ice, and the aquifer-related groundwater recharge factor. Like in calibration basins,  
25 the regionalized parameter values are constrained to the range 0.1 to 5.0. CFA and CFS are  
26 not regionalized but are set to 1.0 in uncalibrated basins.

## 1 **Appendix C**

### 2 **Description of water use models**

3 In pre-processing steps to the WGHM, the global water use sub-models (left side of Fig. 1)  
4 provide water withdrawal and water consumption (the part of withdrawn water that is not  
5 returned to the system but evaporated or incorporated in products) for five sectors: irrigation,  
6 livestock farming, domestic use (households and small businesses), manufacturing industries  
7 and thermal power plant cooling.

8 Irrigation water consumption is calculated on daily time steps for each grid cell by the Global  
9 Irrigation Model (GIM) on the basis of gridded area equipped for irrigation (Siebert et al.,  
10 2005, 2007) and climate as full irrigation (the difference between potential evapotranspiration  
11 and effective precipitation) of paddy rice and non-rice crops, based on modelled cropping  
12 patterns (Döll and Siebert, 2002). Consumptive livestock water use is calculated as a function  
13 of animal numbers per grid cell and water requirements per capita for ten different livestock  
14 types, while national values of domestic and manufacturing water use are downscaled to the  
15 grid cells using population density (Flörke et al., 2013). Cooling water use per grid cell  
16 accounts for the location of more than 60 000 power plants, their cooling and combustion  
17 type, and their electricity production (Flörke et al., 2013; Vassolo and Döll, 2005). Temporal  
18 development of domestic, manufacturing, and cooling water use is calculated as water use  
19 intensity per capita or unit industrial output (considering structural and technological change  
20 over time), multiplied by the driving force of water use, either population (for domestic use),  
21 national manufacturing output (as Gross Value Added, which is a share of Gross Domestic  
22 Product), or national thermal electricity production (Flörke et al., 2013). While WGHM uses  
23 aggregated monthly time series of irrigation consumptive use, the other sectoral water uses  
24 are distributed equally throughout the year.

## 25 **Appendix D**

### 26 **Description of GWSWUSE**

27 In the water use models, the source of the abstracted water is not distinguished. This is done  
28 in the WaterGAP submodel GWSWUSE (Döll et al., 2012). Based on the results of the water  
29 use models, GWSWUSE computes net abstractions (abstractions minus return flows) from

1 groundwater and net abstraction from surface water bodies that serve as input to WGHM (Fig.  
2 1). As a first step within GWSWUSE, the time series of consumptive water use in irrigation,  
3 which is computed by GIM for temporally constant irrigation areas but changing climate  
4 variables, is scaled by using an annual time series of irrigated area by country uses  
5 information (Döll et al., 2012). Then, groundwater use fractions for irrigation (Siebert et al.,  
6 2010), domestic and manufacturing water use are applied, and irrigation water abstractions  
7 are determined by dividing consumptive use by irrigation water use efficiencies. In contrast to  
8 Döll et al. (2012), irrigation water use efficiencies differ between surface water and  
9 groundwater use in WaterGAP 2.2. While for surface water irrigation, country-specific values  
10 are still used, irrigation water use efficiency was set to 0.7 worldwide in case of groundwater  
11 irrigation (Döll et al., 2014). Return flows from irrigation to either groundwater or surface  
12 water are computed as a function of cell-specific artificial drainage fraction (Döll et al., 2012).  
13 In WaterGAP 2.2., the fraction of irrigation return flows that recharge groundwater was  
14 increased as compared to Döll et al. (2012) and is computed as 0.95-0.75 times the cell-  
15 specific artificial drainage fraction. Due to return flows, net abstractions can be positive  
16 (water is abstracted from storage) or negative (water is added to storage) (see Fig. 1 of Döll et  
17 al., 2014).

18

1 **Acknowledgements**

2 The authors thank the Global Runoff Data Center, 56068 Koblenz, Germany for providing the  
3 discharge data used in this study. The authors acknowledge the comments and helpful  
4 suggestions of two anonymous referees that helped to improve the manuscript significantly.

5

## 1 References

- 2 Adam, J. C. and Lettenmaier, D. P.: Adjustment of global gridded precipitation for systematic  
3 bias, *J. Geophys. Res.*, 108, 4257, doi:10.1029/2002JD002499, 2003.
- 4 Alcamo, J., Leemans, R. and Kreileman, E. (Eds.): *Global Change Scenarios of the 21st*  
5 *Century - Results from the IMAGE 2.1 Model*, Pergamon, Oxford., 1998.
- 6 Alcamo, J., Döll, P., Henrichs, T., Kaspar, F., Lehner, B., Rösch, T. and Siebert, S.:  
7 Development and testing of the WaterGAP 2 global model of water use and availability,  
8 *Hydrolog. Sci. J.*, 48, 317–337, doi:10.1623/hysj.48.3.317.45290, 2003.
- 9 Batjes, N. H.: Development of a world data set of soil water retention properties using  
10 pedotransfer rules, *Geoderma*, 71, 31–52, doi:10.1016/0016-7061(95)00089-5, 1996.
- 11 Baumgartner, A. and Reichel, E.: *The World Water Balance: Mean Annual Global,*  
12 *Continental and Maritime Precipitation, Evaporation and Runoff*, Elsevier, Amsterdam, 1975.
- 13 Bergström, S.: The HBV model, in *Computer Models of Watershed Hydrology*, edited by  
14 Singh, V. P., 443–476, Water Resources Publications, Lone Tree, USA, 1995.
- 15 Beven, K. J.: *Rainfall-Runoff Modelling. The Primer*, John Wiley & Sons Ltd., Chichester,  
16 2001.
- 17 Beven, K. J. and Cloke, H. L.: Comment on “Hyperresolution global land surface modeling:  
18 Meeting a grand challenge for monitoring Earth’s terrestrial water” by Eric F. Wood et al.,  
19 *Water Resour. Res.*, 48, W01801, doi:10.1029/2011WR010982, 2012.
- 20 Biemans, H., Hutjes, R. W. A., Kabat, P., Strengers, B. J., Gerten, D. and Rost, S.: Effects of  
21 precipitation uncertainty on discharge calculations for main river basins, *J. Hydrometeorol.*,  
22 10, 1011–1025, doi:10.1175/2008JHM1067.1, 2009.
- 23 Bondeau, A., Smith, P. C., Zaehle, S., Schaphoff, S., Lucht, W., Cramer, W., Gerten, D.,  
24 Lotze-Campen, H., Müller, C., Reichstein, M. and Smith, B.: Modelling the role of  
25 agriculture for the 20<sup>th</sup> century global terrestrial carbon balance, *Glob. Chang. Biol.*, 13, 679-  
26 706, doi:10.1111/j.1365-2486.2006.01305.x, 2007.
- 27 Butts, M. B., Payne, J. T., Kristensen, M. and Madsen, H.: An evaluation of the impact of  
28 model structure on hydrological modelling uncertainty for streamflow simulation, *J. Hydrol.*,  
29 298, 242–266, doi:10.1016/j.jhydrol.2004.03.042, 2004.
- 30 Clark, M. P., Slater, A. G., Rupp, D. E., Woods, R. A., Vrugt, J. A., Gupta, H. V., Wagener,  
31 T. and Hay, L. E.: Framework for Understanding Structural Errors (FUSE): a modular  
32 framework to diagnose differences between hydrological models, *Water Resour. Res.*, 44,  
33 W00B02, doi:10.1029/2007WR006735, 2008.

- 1 Collins, M., Booth, B. B. B, Harris, G. R., Murphy, J. M., Sexton, D. M. H. and Webb, M. J.:  
2 Towards quantifying uncertainty in transient climate change, *Clim. Dyn.* 127–147,  
3 doi:10.1007/s00382-006-0121-0, 2006.
- 4 Corzo Perez, G. A., van Huijgevoort, M. H. J., Voß, F. and van Lanen, H. A. J.: On the  
5 spatio-temporal analysis of hydrological droughts from global hydrological models, *Hydrol.*  
6 *Earth Syst. Sci.*, 15, 2963–2978, doi:10.5194/hess-15-2963-2011, 2011.
- 7 Cowan, W.: Estimating hydraulic roughness coefficients, *Agr. Eng.*, 37, 473–475, 1956.
- 8 Dai, A. and Trenberth, K. E.: Estimates of freshwater discharge from continents: latitudinal  
9 and seasonal variations, *J. Hydrometeorol.*, 3, 660–687, doi:10.1175/1525-  
10 7541(2002)003<0660:EOFDFC>2.0.CO;2, 2002.
- 11 Deardorff, J. W.: Efficient prediction of ground surface temperature and moisture, with  
12 inclusion of a layer of vegetation, *J. Geophys. Res.*, 83, 1889, doi:10.1029/JC083iC04p01889,  
13 1978.
- 14 Dee, D. P., Uppala, S. M., Simmons, A. J., Berrisford, P., Poli, P., Kobayashi, S., Andrae, U.,  
15 Balmaseda, M. A., Balsamo, G., Bauer, P., Bechtold, P., Beljaars, A. C. M., van de Berg, L.,  
16 Bidlot, J., Bormann, N., Delsol, C., Dragani, R., Fuentes, M., Geer, A. J., Haimberger, L.,  
17 Healy, S. B., Hersbach, H., Hólm, E. V., Isaksen, L., Kållberg, P., Köhler, M., Matricardi, M.,  
18 McNally, A. P., Monge-Sanz, B. M., Morcrette, J.-J., Park, B.-K., Peubey, C., de Rosnay, P.,  
19 Tavolato, C., Thépaut, J.-N. and Vitart, F.: The ERA-Interim reanalysis: configuration and  
20 performance of the data assimilation system, *Q. J. R. Meteorol. Soc.*, 137(656), 553–597,  
21 doi:10.1002/qj.828, 2011.
- 22 Döll, P. and Fiedler, K.: Global-scale modeling of groundwater recharge, *Hydrol. Earth Syst.*  
23 *Sci.*, 12, 863–885, doi:10.5194/hess-12-863-2008, 2008.
- 24 Döll, P. and Lehner, B.: Validation of a new global 30-min drainage direction map, *J.*  
25 *Hydrol.*, 258, 214–231, doi:10.1016/S0022-1694(01)00565-0, 2002.
- 26 Döll, P. and Müller Schmied, H.: How is the impact of climate change on river flow regimes  
27 related to the impact on mean annual runoff? A global-scale analysis, *Environ. Res. Lett.*, 7,  
28 014037, doi:10.1088/1748-9326/7/1/014037, 2012.
- 29 Döll, P. and Siebert, S.: Global modeling of irrigation water requirements, *Water Resour.*  
30 *Res.*, 38, 8-1–8-10, doi:10.1029/2001WR000355, 2002.
- 31 Döll, P., Kaspar, F. and Lehner, B.: A global hydrological model for deriving water  
32 availability indicators: model tuning and validation, *J. Hydrol.*, 270, 105–134,  
33 doi:10.1016/S0022-1694(02)00283-4, 2003.
- 34 Döll, P., Fiedler, K. and Zhang, J.: Global-scale analysis of river flow alterations due to water  
35 withdrawals and reservoirs, *Hydrol. Earth Syst. Sci.*, 13, 2413–2432, doi:10.5194/hess-13-  
36 2413-2009, 2009.

- 1 Döll, P., Fritsche, M., Eicker, A. and Müller Schmied, H.: Seasonal water storage variations  
2 as impacted by water abstractions: comparing the output of a global hydrological model with  
3 GRACE and GPS observations, *Surv. Geophys.*, doi:10.1007/s10712-014-9282-2, 2014.
- 4 Döll, P., Müller Schmied, H., Schuh, C., Portmann, F. T. and Eicker, A.: Global-scale  
5 assessment of groundwater depletion and related groundwater abstractions: Combining  
6 hydrological modeling with information from well observations and GRACE satellites, *Water*  
7 *Resour. Res.*, 50, doi:10.1002/2014WR015595, 2014.
- 8 Döll, P., Hoffmann-Dobrev, H., Portmann, F. T., Siebert, S., Eicker, A., Rodell, M.,  
9 Strassberg, G. and Scanlon, B. R.: Impact of water withdrawals from groundwater and surface  
10 water on continental water storage variations, *J. Geodyn.*, 59-60, 143–156,  
11 doi:10.1016/j.jog.2011.05.001, 2012.
- 12 European Environment Agency: Corine land cover 2000: mapping a decade of change,  
13 Copenhagen, 2004.
- 14 Fekete, B. M., Vörösmarty, C. J. and Grabs, W.: High-resolution fields of global runoff  
15 combining observed river discharge and simulated water balances, *Global Biogeochem. Cy.*,  
16 16, 15-1–15-10, doi:10.1029/1999GB001254, 2002.
- 17 Flörke, M., Kynast, E., Bärlund, I., Eisner, S., Wimmer, F. and Alcamo, J.: Domestic and  
18 industrial water uses of the past 60 years as a mirror of socio-economic development: A  
19 global simulation study, *Glob. Environ. Chang.*, 23, 144–156,  
20 doi:10.1016/j.gloenvcha.2012.10.018, 2013.
- 21 Gosling, S. N. and Arnell, N. W.: Simulating current global river runoff with a global  
22 hydrological model: model revisions, validation, and sensitivity analysis, *Hydrol. Process.*,  
23 25, 1129–1145, doi:10.1002/hyp.7727, 2011.
- 24 Gudmundsson, L., Tallaksen, L., Stahl, K., Clark, D., Dumont, E., Hagemann, S., Bertrand,  
25 N., Gerten, D., Heinke, J., Hanasaki, N., Voss, F. and Koirala, S.: Comparing large-scale  
26 hydrological model simulations to observed runoff percentiles in Europe, *J. Hydrometeorol.*,  
27 13, 604–620, doi:10.1175/JHM-D-11-083.1, 2012a.
- 28 Gudmundsson, L., Wagener, T., Tallaksen, L. M. and Engeland, K.: Evaluation of nine large-  
29 scale hydrological models with respect to the seasonal runoff climatology in Europe, *Water*  
30 *Resour. Res.*, 48, 1–20, doi:10.1029/2011WR010911, 2012b.
- 31 Güntner, A., Stuck, J., Werth, S., Döll, P., Verzano, K. and Merz, B.: A global analysis of  
32 temporal and spatial variations in continental water storage, *Water Resour. Res.*, 43, W05416,  
33 doi:10.1029/2006WR005247, 2007.
- 34 Guo, Z., Dirmeyer, P. A., Hu, Z.-Z., Gao, X. and Zhao, M.: Evaluation of the second global  
35 soil wetness project soil moisture simulations: 2. Sensitivity to external meteorological  
36 forcing, *J. Geophys. Res.*, 111, D22S03, doi:10.1029/2006JD007845, 2006.
- 37 Haddeland, I., Clark, D. B., Franssen, W., Ludwig, F., Voß, F., Arnell, N. W., Bertrand, N.,  
38 Best, M., Folwell, S., Gerten, D., Gomes, S., Gosling, S. N., Hagemann, S., Hanasaki, N.,

- 1 Harding, R., Heinke, J., Kabat, P., Koirala, S., Oki, T., Polcher, J., Stacke, T., Viterbo, P.,  
2 Weedon, G. P. and Yeh, P.: Multimodel estimate of the global terrestrial water balance: setup  
3 and first results, *J. Hydrometeorol.*, 12, 869–884, doi:10.1175/2011JHM1324.1, 2011.
- 4 Hagemann, S., Chen, C., Clark, D. B., Folwell, S., Gosling, S. N., Haddeland, I., Hanasaki,  
5 N., Heinke, J., Ludwig, F., Voss, F. and Wiltshire, A. J.: Climate change impact on available  
6 water resources obtained using multiple global climate and hydrology models, *Earth Syst.*  
7 *Dyn.*, 4, 129–144, doi:10.5194/esd-4-129-2013, 2013.
- 8 Hanasaki, N., Kanae, S. and Oki, T.: A reservoir operation scheme for global river routing  
9 models, *J. Hydrol.*, 327, 22–41, doi:10.1016/j.jhydrol.2005.11.011, 2006.
- 10 Hanasaki, N., Kanae, S., Oki, T., Masuda, K., Motoya, K., Shirakawa, N., Shen, Y. and  
11 Tanaka, K.: An integrated model for the assessment of global water resources – Part 1: Model  
12 description and input meteorological forcing, *Hydrol. Earth Syst. Sci.*, 12, 1007–1025,  
13 doi:10.5194/hess-12-1007-2008, 2008.
- 14 Harris, I., Jones, P. D., Osborn, T. J. and Lister, D. H.: Updated high-resolution grids of  
15 monthly climatic observations - the CRU TS3.10 Dataset, *Int. J. Climatol.*, 34, 623–642,  
16 doi:10.1002/joc.3711, 2014.
- 17 Hoekstra, A. Y., Mekonnen, M. M., Chapagain, A. K., Mathews, R. E. and Richter, B. D.:  
18 Global monthly water scarcity: blue water footprints versus blue water availability, *PLoS*  
19 *One*, 7, e32688, doi:10.1371/journal.pone.0032688, 2012.
- 20 Hunger, M. and Döll, P.: Value of river discharge data for global-scale hydrological  
21 modeling, *Hydrol. Earth Syst. Sci.*, 12, 841–861, doi:10.5194/hess-12-841-2008, 2008.
- 22 Jasechko, S., Sharp, Z. D., Gibson, J. J., Birks, S. J., Yi, Y. and Fawcett, P. J.: Terrestrial  
23 water fluxes dominated by transpiration., *Nature*, 496, 347–350, doi:10.1038/nature11983,  
24 2013.
- 25 Jung, M., Reichstein, M., Ciais, P., Seneviratne, S. I., Sheffield, J., Goulden, M. L., Bonan,  
26 G., Cescatti, A., Chen, J., de Jeu, R., Dolman, A. J., Eugster, W., Gerten, D., Gianelle, D.,  
27 Gobron, N., Heinke, J., Kimball, J., Law, B. E., Montagnani, L., Mu, Q., Mueller, B., Oleson,  
28 K., Papale, D., Richardson, A. D., Roupsard, O., Running, S., Tomelleri, E., Viovy, N.,  
29 Weber, U., Williams, C., Wood, E., Zaehle, S. and Zhang, K.: Recent decline in the global  
30 land evapotranspiration trend due to limited moisture supply., *Nature*, 467, 951–954,  
31 doi:10.1038/nature09396, 2010.
- 32 Kaspar, F.: Entwicklung und Unsicherheitsanalyse eines globalen hydrologischen Modells,  
33 Ph.D. thesis, University of Kassel, Germany, 2003.
- 34 Koirala, S., Yeh, P. J.-F., Hirabayashi, Y., Kanae, S. and Oki, T.: Global-scale land surface  
35 hydrologic modeling with the representation of water table dynamics, *J. Geophys. Res.*  
36 *Atmos.*, 119, 75–89, doi:10.1002/2013JD020398, 2014.
- 37 Korzun, V. I.: World water balance and water resources of the world, *UNESCO Stud. Reports*  
38 *Hydrol.*, 25, 663, 1978.



- 1 Kottek, M., Grieser, J., Beck, C., Rudolf, B. and Rubel, F.: World map of the Koppen-Geiger  
2 climate classification updated, *Meteorol. Z.*, 15, 259–263, doi:10.1127/0941-2948/2006/0130,  
3 2006.
- 4 Legates, D. R.: A climatology of global precipitation, *Publ. Climatol.*, 40, University of  
5 Delaware, Newark, USA 1987.
- 6 Lehner, B. and Döll, P.: Development and validation of a global database of lakes, reservoirs  
7 and wetlands, *J. Hydrol.*, 296, 1–22, doi:10.1016/j.jhydrol.2004.03.028, 2004.
- 8 Lehner, B., Verdin, K. and Jarvis, A.: New global hydrography derived from spaceborne  
9 elevation data, *Eos T. Am. Geophys. Un.*, 89, 93, doi:10.1029/2008EO100001, 2008.
- 10 Lehner, B., Liermann, C. R., Revenga, C., Vörösmarty, C., Fekete, B., Crouzet, P., Döll, P.,  
11 Endejan, M., Frenken, K., Magome, J., Nilsson, C., Robertson, J. C., Rödel, R., Sindorf, N.  
12 and Wisser, D.: High-resolution mapping of the world's reservoirs and dams for sustainable  
13 river-flow management, *Front. Ecol. Environ.*, 9, 494–502, doi:10.1890/100125, 2011.
- 14 Maniak, U.: *Hydrologie und Wasserbewirtschaftung*, 4th Edn., Springer, Berlin, 1997.
- 15 Masaki, Y., Hanasaki, N., Takahashi, K. and Hijioka, Y.: Global-scale analysis on future  
16 changes in flow regimes using Gini and Lorenz asymmetry coefficients, *Water Resour. Res.*,  
17 50, doi:10.1002/2013WR014266, 2014.
- 18 Miralles, D. G., Holmes, T. R. H., De Jeu, R. A. M., Gash, J. H., Meesters, A. G. C. A. and  
19 Dolman, A. J.: Global land-surface evaporation estimated from satellite-based observations,  
20 *Hydrol. Earth Syst. Sci.*, 15, 453–469, doi:10.5194/hess-15-453-2011, 2011.
- 21 Mu, Q., Zhao, M. and Running, S. W.: Improvements to a MODIS global terrestrial  
22 evapotranspiration algorithm, *Remote Sens. Environ.*, 115, 1781–1800,  
23 doi:10.1016/j.rse.2011.02.019, 2011.
- 24 Mueller, B., Seneviratne, S. I., Jimenez, C., Corti, T., Hirschi, M., Balsamo, G., Ciais, P.,  
25 Dirmeyer, P., Fisher, J. B., Guo, Z., Jung, M., Maignan, F., McCabe, M. F., Reichle, R.,  
26 Reichstein, M., Rodell, M., Sheffield, J., Teuling, A. J., Wang, K., Wood, E. F. and Zhang,  
27 Y.: Evaluation of global observations-based evapotranspiration datasets and IPCC AR4  
28 simulations, *Geophys. Res. Lett.*, 38, L06402, doi:10.1029/2010GL046230, 2011.
- 29 Mueller, B., Hirschi, M., Jimenez, C., Ciais, P., Dirmeyer, P. A., Dolman, A. J., Fisher, J. B.,  
30 Jung, M., Ludwig, F., Maignan, F., Miralles, D. G., McCabe, M. F., Reichstein, M., Sheffield,  
31 J., Wang, K., Wood, E. F., Zhang, Y. and Seneviratne, S. I.: Benchmark products for land  
32 evapotranspiration: LandFlux-EVAL multi-data set synthesis, *Hydrol. Earth Syst. Sci.*, 17,  
33 3707–3720, doi:10.5194/hess-17-3707-2013, 2013.
- 34 Nash, J. and Sutcliffe, J.: River flow forecasting through conceptual models part I: A  
35 discussion of principles, *J. Hydrol.*, 10, 282–290, 1970.
- 36 Nijssen, B., O'Donnell, G. M., Lettenmaier, D. P., Lohmann, D. and Wood, E. F.: Predicting  
37 the discharge of global rivers, *J. Climate*, 14, 3307–3323, 2001.

- 1 Oki, T. and Kanae, S.: Global hydrological cycles and world water resources, *Science*, 313,  
2 1068–72, doi:10.1126/science.1128845, 2006.
- 3 Pokhrel, Y., Hanasaki, N., Koirala, S., Cho, J., Yeh, P. J.-F., Kim, H., Kanae, S. and Oki, T.:  
4 Incorporating anthropogenic water regulation modules into a land surface model, *J.*  
5 *Hydrometeorol.*, 13, 255–269, doi:10.1175/JHM-D-11-013.1, 2012.
- 6 Portmann, F. T., Döll, P., Eisner, S. and Flörke, M.: Impact of climate change on renewable  
7 groundwater resources: assessing the benefits of avoided greenhouse gas emissions using  
8 selected CMIP5 climate projections, *Environ. Res. Lett.*, 8, 024023, doi:10.1088/1748-  
9 9326/8/2/024023, 2013.
- 10 Priestley, C. H. B. and Taylor, R. J.: Assessment of surface heat flux and evaporation using  
11 large-scale parameters, *Mon. Weather Rev.*, 100, 81–92, doi:10.1175/1520-  
12 0493(1972)100<0081:OTAOSH>2.3.CO;2, 1972.
- 13 Prudhomme, C., Parry, S., Hannaford, J., Clark, D. B., Hagemann, S. and Voss, F.: How well  
14 do large-scale models reproduce regional hydrological extremes in Europe?, *J.*  
15 *Hydrometeorol.*, 12, 1181–1204, doi:10.1175/2011JHM1387.1, 2011.
- 16 Prudhomme, C., Giuntoli, I., Robinson, E. L., Clark, D. B., Arnell, N. W., Dankers, R.,  
17 Fekete, B. M., Franssen, W., Gerten, D., Gosling, S. N., Hagemann, S., Hannah, D. M., Kim,  
18 H., Masaki, Y., Satoh, Y., Stacke, T., Wada, Y. and Wisser, D.: Hydrological droughts in the  
19 21st century, hotspots and uncertainties from a global multimodel ensemble experiment., *P.*  
20 *Natl. Acad. Sci. U. S. A.*, 111, 3262–7, doi:10.1073/pnas.1222473110, 2014.
- 21 Refsgaard, J. C., van der Sluijs, J. P., Brown, J. and van der Keur, P.: A framework for  
22 dealing with uncertainty due to model structure error, *Adv. Water Resour.*, 29, 1586–1597,  
23 doi:10.1016/j.advwatres.2005.11.013, 2006.
- 24 Rowlands, D. J., Frame, D. J., Ackerley, D., Aina, T., Booth, B. B. B., Christensen, C.,  
25 Collins, M., Faull, N., Forest, C. E., Grandey, B. S., Gryspeerdt, E., Highwood, E. J., Ingram,  
26 W. J., Knight, S., Lopez, A., Massey, N., Mcnamara, F., Meinshausen, N., Piani, C., Rosier,  
27 S. M., Sanderson, B. M., Smith, L. A., Stone, D. A., Thurston, M., Yamazaki, K., Yamazaki,  
28 Y. H. and Allen, M. R.: Broad range of 2050 warming from an observationally constrained  
29 large climate model ensemble, *Nat. Geosci.*, 5, 256–260, doi:10.1038/ngeo1430, 2012.
- 30 Schewe, J., Heinke, J., Gerten, D., Haddeland, I., Arnell, N. W., Clark, D. B., Dankers, R.,  
31 Eisner, S., Fekete, B. M., Colón-González, F. J., Gosling, S. N., Kim, H., Liu, X., Masaki, Y.,  
32 Portmann, F. T., Satoh, Y., Stacke, T., Tang, Q., Wada, Y., Wisser, D., Albrecht, T., Frieler,  
33 K., Piontek, F., Warszawski, L. and Kabat, P.: Multimodel assessment of water scarcity under  
34 climate change., *P. Natl. Acad. Sci. U. S. A.*, 111, 3245–50, doi:10.1073/pnas.1222460110,  
35 2014.
- 36 Schmidt, R., Schwintzer, P., Flechtner, F., Reigber, C., Güntner, A., Döll, P., Ramillien, G.,  
37 Cazenave, A., Petrovic, S., Jochmann, H. and Wunsch, J.: GRACE observations of changes in  
38 continental water storage, *Global Planet. Change*, 50, 112–126,  
39 doi:10.1016/j.gloplacha.2004.11.018, 2006.

- 1 Schneider, C., Flörke, M., Eisner, S. and Voss, F.: Large scale modelling of bankfull flow: an  
2 example for Europe, *J. Hydrol.*, 408, 235–245, doi:10.1016/j.jhydrol.2011.08.004, 2011.
- 3 Schneider, U., Becker, A., Finger, P., Meyer-Christoffer, A., Ziese, M. and Rudolf, B.:  
4 GPCC's new land surface precipitation climatology based on quality-controlled in situ data  
5 and its role in quantifying the global water cycle, *Theor. Appl. Climatol.*, 115, 15–40,  
6 doi:10.1007/s00704-013-0860-x, 2014.
- 7 Schulze, E. D., Kelliher, F. M., Korner, C., Lloyd, J. and Leuning, R.: Relationships among  
8 maximum stomatal conductance, ecosystem surface conductance, carbon assimilation rate,  
9 and plant nitrogen nutrition: A global ecology scaling exercise, *Annu. Rev. Ecol. Syst.*, 25,  
10 629–662, doi:10.1146/annurev.es.25.110194.003213, 1994.
- 11 Schulze, K. and Döll, P.: Neue Ansätze zur Modellierung von Schneeakkumulation und -  
12 schmelze im globalen Wassermmodell WaterGAP, in: Tagungsband zum 7. Workshop zur  
13 großskaligen Modellierung in der Hydrologie, edited by: Ludwig, R., Reichert, D. and  
14 Mauser, W., Kassel University Press, Kassel, 2004.
- 15 Schumacher, M., Eicker, A., Kusche, J., Müller Schmied, H. and Döll, P.: Covariance  
16 analysis and sensitivity studies for GRACE assimilation into WGHM, in: IAG Symposia  
17 Series: Proceedings of the IAG Scientific Assembly 2013, (accepted), 2014.
- 18 Scurlock, J. M., Asner, G. P. and Gower, S. T.: Worldwide Historical Estimates of Leaf Area  
19 Index, 1932-2000, Oak Ridge National Library, Oak Ridge, USA, 2001.
- 20 Shuttleworth, W. J.: Evaporation, in *Handbook of Hydrology*, edited by: Maidment, D. R.,  
21 McGraw-Hill, New York, 4.1–4.53, 1993.
- 22 Siebert, S., Döll, P., Hoogeveen, J., Faures, J.-M., Frenken, K. and Feick, S.: Development  
23 and validation of the global map of irrigation areas, *Hydrol. Earth Syst. Sci.*, 9, 535–547,  
24 doi:10.5194/hess-9-535-2005, 2005.
- 25 Siebert, S., Döll, P., Feick, S., Hoogeveen, J. and Frenken, K.: Global map of irrigation areas  
26 version 4.0.1, [CD-ROM], FAO Land and Water Digital Media Series (34), Rome, Italy,  
27 FAO, 2007.
- 28 Siebert, S., Burke, J., Faures, J. M., Frenken, K., Hoogeveen, J., Döll, P. and Portmann, F. T.:  
29 Groundwater use for irrigation – a global inventory, *Hydrol. Earth Syst. Sci.*, 14, 1863–1880,  
30 doi:10.5194/hess-14-1863-2010, 2010.
- 31 Song, X., Zhan, C., Kong, F. and Xia, J.: Advances in the study of uncertainty quantification  
32 of large-scale hydrological modeling system, *J. Geogr. Sci.*, 21, 801–819,  
33 doi:10.1007/s11442-011-0881-2, 2011.
- 34 Sperna Weiland, F. C., van Beek, L. P. H., Kwadijk, J. C. J. and Bierkens, M. F. P.: The  
35 ability of a GCM-forced hydrological model to reproduce global discharge variability,  
36 *Hydrol. Earth Syst. Sci.*, 14, 1595–1621, doi:10.5194/hess-14-1595-2010, 2010.

- 1 Sterling, S. M., Ducharne, A. and Polcher, J.: The impact of global land-cover change on the  
2 terrestrial water cycle, *Nat. Clim. Chang.*, 3, 385–390, doi:10.1038/nclimate1690, 2012.
- 3 Thompson, J. R., Green, A. J., Kingston, D. G. and Gosling, S. N.: Assessment of uncertainty  
4 in river flow projections for the Mekong River using multiple GCMs and hydrological  
5 models, *J. Hydrol.*, 486, 1–30, doi:10.1016/j.jhydrol.2013.01.029, 2013.
- 6 UNEP: *World Atlas of Desertification*, Edward Arnold, Sevenoaks, 1992.
- 7 US Geological Survey: GTOPO30 Digital Elevation Model, available at:  
8 [http://webmap.ornl.gov/wcsdown/dataset.jsp?ds\\_id=10003](http://webmap.ornl.gov/wcsdown/dataset.jsp?ds_id=10003) (last access: 12 December 2013),  
9 2003.
- 10 USGS: Global Land Cover Characterization, available at: <http://edc2.usgs.gov/glcc/glcc.php>  
11 (last access: 22 October 2012), 2008.
- 12 Van Beek, L. P. H., Wada, Y. and Bierkens, M. F. P.: Global monthly water stress: 1. Water  
13 balance and water availability, *Water Resour. Res.*, 47, W07517,  
14 doi:10.1029/2010WR009791, 2011.
- 15 Van Loon, A. F., Van Huijgevoort, M. H. J. and Van Lanen, H. A. J.: Evaluation of drought  
16 propagation in an ensemble mean of large-scale hydrological models, *Hydrol. Earth Syst.  
17 Sci.*, 16, 4057–4078, doi:10.5194/hess-16-4057-2012, 2012.
- 18 Vassolo, S. and Döll, P.: Global-scale gridded estimates of thermoelectric power and  
19 manufacturing water use, *Water Resour. Res.*, 41, W04010, doi:10.1029/2004WR003360,  
20 2005.
- 21 Verzano, K., Bärlund, I., Flörke, M., Lehner, B., Kynast, E., Voß, F. and Alcamo, J.:  
22 Modeling variable river flow velocity on continental scale: current situation and climate  
23 change impacts in Europe, *J. Hydrol.*, 424–425, 238–251, doi:10.1016/j.jhydrol.2012.01.005,  
24 2012.
- 25 Vinukollu, R. K., Wood, E. F., Ferguson, C. R. and Fisher, J. B.: Global estimates of  
26 evapotranspiration for climate studies using multi-sensor remote sensing data: evaluation of  
27 three process-based approaches, *Remote Sens. Environ.*, 115, 801–823,  
28 doi:10.1016/j.rse.2010.11.006, 2011.
- 29 Vörösmarty, C., Federer, C. and Schloss, A.: Potential evaporation functions compared on US  
30 watersheds: possible implications for global-scale water balance and terrestrial ecosystem  
31 modeling, *J. Hydrol.*, 207, 147–169, doi:10.1016/S0022-1694(98)00109-7, 1998.
- 32 Wada, Y., van Beek, L. P. H., van Kempen, C. M., Reckman, J. W. T. M., Vasak, S. and  
33 Bierkens, M. F. P.: Global depletion of groundwater resources, *Geophys. Res. Lett.*, 37,  
34 L20402, doi:10.1029/2010GL044571, 2010.
- 35 Wang, K. and Liang, S.: An improved method for estimating global evapotranspiration based  
36 on satellite determination of surface net radiation, vegetation index, temperature, and soil  
37 moisture, *J. Hydrometeorol.*, 9, 712–727, doi:10.1175/2007JHM911.1, 2008.

- 1    Warszawski, L., Frieler, K., Huber, V., Piontek, F., Serdeczny, O., and Schewe, J.: The Inter-  
2    Sectoral Impact Model Intercomparison Project (ISI-MIP): project framework, *Proc. Natl.*  
3    *Acad. Sci. U. S. A.*, 111(9), 3228-32, doi:10.1073/pnas.1312330110, 2014.
- 4    Weedon, G. P., Gomes, S., Viterbo, P., Österle, H., Adam, J. C., Bellouin, N., Boucher, O.  
5    and Best, M.: The WATCH Forcing Data: a meteorological forcing dataset for land surface-  
6    and hydrological models, *Watch Techn. Rep.*, 22, (available at: [www.eu-](http://www.eu-watch.org/publications)  
7    [watch.org/publications](http://www.eu-watch.org/publications)), 2010.
- 8    Weedon, G. P., Gomes, S., Viterbo, P., Shuttleworth, W. J., Blyth, E., Österle, H., Adam, J.  
9    C., Bellouin, N., Boucher, O. and Best, M.: Creation of the WATCH Forcing Data and its use  
10   to assess global and regional reference crop evaporation over land during the twentieth  
11   century, *J. Hydrometeorol.*, 12, 823–848, doi:10.1175/2011JHM1369.1, 2011.
- 12   Werth, S. and Güntner, A.: Calibration analysis for water storage variability of the global  
13   hydrological model WGHM, *Hydrol. Earth Syst. Sci.*, 14, 59–78, doi:10.5194/hess-14-59-  
14   2010, 2010.
- 15   Widén-Nilsson, E., Halldin, S. and Xu, C.: Global water-balance modelling with WASMOD-  
16   M: parameter estimation and regionalisation, *J. Hydrol.*, 340, 105–118,  
17   doi:10.1016/j.jhydrol.2007.04.002, 2007.
- 18   Wilber, A. C., Kratz, D. P. and Gupta, S. K.: Surface emissivity maps for use in satellite  
19   retrievals of longwave radiation, NASA/TP-1999-209362, Langley Research Center,  
20   Hampton, USA, 1999.
- 21   WMO: Guide to hydrological practices, Geneva, 1994.
- 22   Wood, E. F., Roundy, J. K., Troy, T. J., van Beek, R. L. P. H., Bierkens, M. F. P., Blyth, E.,  
23   de Roo, A., Döll, P., Ek, M., Famiglietti, J., Gochis, D., van de Giesen, N., Houser, P., Jaffé,  
24   P. R., Kollet, S., Lehner, B., Lettenmaier, D. P., Peters-Lidard, C., Sivapalan, M., Sheffield,  
25   J., Wade, A. and Whitehead, P.: Hyperresolution global land surface modeling: meeting a  
26   grand challenge for monitoring Earth’s terrestrial water, *Water Resour. Res.*, 47, W05301,  
27   doi:10.1029/2010WR010090, 2011.
- 28   Wood, E. F., Roundy, J. K., Troy, T. J., van Beek, R. L. P. H., Bierkens, M. F. P., Blyth, E.,  
29   de Roo, A., Döll, P., Ek, M., Famiglietti, J., Gochis, D., van de Giesen, N., Houser, P., Jaffe,  
30   P., Kollet, S., Lehner, B., Lettenmaier, D. P., Peters-Lidard, C. D., Sivapalan, M., Sheffield,  
31   J., Wade, A. J. and Whitehead, P.: Reply to comment by Keith J. Beven and Hannah L. Cloke  
32   on “Hyperresolution global land surface modeling: meeting a grand challenge for monitoring  
33   Earth’s terrestrial water,” *Water Resour. Res.*, 48, W01802, doi:10.1029/2011WR011202,  
34   2012.
- 35
- 36

1 Table 1. Overview of the model variants.

Name	Characteristic	Description
STANDARD	standard WaterGAP 2.2 model version	MODIS land cover for the year 2004. WATCH Forcing Data as daily climate input. For 1901-1978 WFD is used, for 1979-2009 WFDEI. Calibration against mean annual river discharge, including regionalization of calibration parameter to grid cells outside calibration basins. Consideration of human water use.
CLIMATE	alternative climate forcing	Similar to STANDARD but CRU TS 3.2 and GPCC v6 for precipitation as monthly climate input.
LANDCOVER	alternative land cover data	Similar to STANDARD but a combination of GLCC and CORINE (for Europe) was used as land cover input.
STRUCTURE	alternative model structure	Similar to STANDARD but less refined process representation (comparable to Döll et al. (2003)).
NoUse	no water use	Similar to STANDARD but without considering water use.
NoCal	no calibration	Similar to STANDARD but without calibration to mean annual river discharge. Calibration parameter and correction factors are globally set to 1.0 (for details see Appendix B)

2

3

1 Table 2. Long-term average (1971-2000) freshwater fluxes from global land area (except  
2 Antarctica and Greenland) of WaterGAP 2.2 in  $\text{km}^3 \text{ yr}^{-1}$ . Cells representing inland sinks were  
3 excluded but discharge into inland sinks was included.

nr	component	STANDARD	NoUse <sup>h</sup>	CLIMATE	LANDCOVER	STRUCTURE	NoCal
1	precipitation P <sup>a</sup>	111 070	111 070	112 969	111 070	111 070	111 070
2	actual evapotranspiration AET <sup>b</sup>	69 803	69 934	69 842	70 012	70 217	63 344
3	discharge into oceans and inland sinks Q <sup>c</sup>	40 458	41 216	42 364	40 250	40 002	46 822
4	water consumption (actual) (rows 5 + 7) WC <sub>a</sub>	1031	0	927	1029	983	1054
5	net abstraction from surface water (actual) <sup>d</sup>	1102	0	960	1102	983	1126
6	net abstraction from surface water (demand) NA <sub>s</sub> <sup>e</sup>	1154	0	1000	1154	1082	1154
7	net abstraction from groundwater NA <sub>g</sub> <sup>f</sup>	-72	0	-33	-72	0	-72
8	change of total water storage dS/dt <sup>g</sup>	-215	-73	-156	-214	-44	-143
9	long term averaged yearly volume balance error (P – AET – Q – WC <sub>a</sub> – dS/dt) deviation to P	-7	-7	-8	-7	-88	-7
		-0.006%	-0.006%	-0.007%	-0.006%	-0.08%	-0.006%

4 <sup>a</sup> mean annual P (1979-2001) is  $110.309 \text{ km}^3 \text{ yr}^{-1}$  in WFD and  $110.812 \text{ km}^3 \text{ yr}^{-1}$  in WFDEI, <sup>b</sup>  
5 AET does not include evapotranspiration caused by human water use, i.e. actual water  
6 consumption WC<sub>a</sub>, <sup>c</sup> including anthropogenic water use (except NoUse), <sup>d</sup> if not enough water  
7 is available, demand is not completely satisfied, <sup>e</sup> demand that needs to be satisfied (water use  
8 model output), <sup>f</sup> negative values indicate that return flows from irrigation with surface water  
9 exceed groundwater abstractions, <sup>g</sup> total water storage (TWS) of 31. December 2000 minus

- 1 TWS of 31. December 1970 divided by 30 years, <sup>h</sup> STANDARD but no subtraction of water
- 2 use; discharge into oceans and inland sinks equals renewable water resources.
- 3



1 Table 3. Mean change in water storage in different compartments between December 31,  
 2 1970, and December 31, 2000, in km<sup>3</sup> yr<sup>-1</sup> (global sum except Antarctica and Greenland).  
 3 Cells representing inland sinks were excluded.

compartment	STANDARD	NoUse <sup>a</sup>	CLIMATE	LANDCOVER	STRUCTURE	NoCal
total water storage	-214.8	-73.7	-156.4	-214.8	-44.5	-143.0
canopy	-0.05	-0.05	0.002	-0.05	-0.05	-0.05
snow	-3.0	-3.0	-6.3	-3.3	-1.3	-3.0
soil	-21.6	-21.6	-0.9	-20.6	-20.9	-20.0
groundwater	-124.9	8.6	-126.9	-125.4	9.7	-82.7
local lake	-1.9	-1.5	-0.3	-1.9	-2.1	-1.1
local wetland	-4.9	-4.3	1.9	-5.1	-8.4	-2.2
global lake	-3.5	-3.4	-1.1	-3.4	-8.2	-3.8
reservoirs	-43.1	-37.5	-23.2	-43.1	*	-21.4
global wetlands	-4.9	-4.3	1.9	-5.1	-8.4	-2.2
river	-6.7	-6.0	2.7	-6.7	-4.6	-4.3

4 <sup>a</sup> In WaterGAP, increase of soil water storage by irrigation is not taken into account such that  
 5 storage values for STANDARD and NoUse variants are the same.

6 \* not applicable as reservoirs are treated as global lakes

7

1 Table 4. Number of calibration basins per  $E_{NS}$  category and Köppen-Geiger climate zone<sup>a</sup>.

Variant	class	$E_{NS}$	A	B	C	D	E	sum
STANDARD	1	> 0.7	75	19	117	129	29	369
	2	0.5 - 0.7	100	17	68	134	18	337
	3	< 0.5	110	91	83	282	47	613
CLIMATE	1	> 0.7	67	8	77	145	30	327
	2	0.5 - 0.7	116	31	68	107	26	348
	3	< 0.5	104	79	127	293	41	644
LANDCOVER	1	> 0.7	77	20	117	128	32	374
	2	0.5 - 0.7	94	16	68	132	15	325
	3	< 0.5	114	91	83	285	47	620
STRUCTURE	1	> 0.7	63	20	85	99	27	294
	2	0.5 - 0.7	101	16	84	132	22	355
	3	< 0.5	121	91	99	314	45	670
NoUse	1	> 0.7	77	15	109	138	30	369
	2	0.5 - 0.7	97	26	68	130	17	338
	3	< 0.5	111	86	91	277	47	612
NoCal	1	> 0.7	17	5	39	61	12	134
	2	0.5 - 0.7	28	4	32	80	11	155
	3	< 0.5	240	118	197	404	71	1030

2 <sup>a</sup> Calculated by WaterGAP after (Kottek et al., 2006); A: equatorial climate, B: arid climate,  
3 C: warm temperate climate, D: snow climate and E: polar climates. Note that the number of  
4 basins per climate zone differs for CLIMATE as here, the basis for Köppen-Geiger climate  
5 calculation is CRU TS 3.2 and GPCC v6 instead of WFD/WFDEI climate input for all other  
6 variants.

7

1 Table 5. Comparison of diverse estimates of global actual evapotranspiration and discharge in  
 2  $\text{km}^3 \text{ yr}^{-1}$ .

actual evapotranspiration		discharge	
62 800	Mu et al. (2011)	34 406	Mueller et al. (2013)
64 512 <sup>a</sup>	Mueller et al. (2013)	36 200	Wada et al. (2010)
65 000	Jung et al. (2010)	36 687	Döll et al. (2003)
65 500	Oki and Kanae (2006)	37 288	Dai and Trenberth (2002)
66 000	Sterling et al. (2012)	38 587	Baumgartner and Reichel (1975)
71 000	Baumgartner and Reichel (1975)	38 605	Widén-Nilsson et al. (2007)
72 000	Korzun (1978)	39 307	Fekete et al. (2002)
75 981 <sup>b</sup>	Mueller et al. (2011)	39 414	Döll and Fiedler (2008)
60 000–	Haddeland et al. (2011)	44 560	Korzun (1978)
85 000		45 500	Oki and Kanae (2006)
		42 000–	Haddeland et al. (2011)
		66 000	
70576 <sup>c</sup>	STANDARD	40458 <sup>c</sup>	STANDARD

3 <sup>a</sup> 1.35 mm d<sup>-1</sup> based on a land area of  $130.922 \times 10^6 \text{ km}^2$

4 <sup>b</sup> 1.59 mm d<sup>-1</sup> based on a land area of  $130.922 \times 10^6 \text{ km}^2$  (value taken from Mueller et al.  
 5 (2013) as no area is given in Mueller et al. (2011))

6 <sup>c</sup> sum of AET and WC<sub>a</sub>

7

1 Table 6. The three model variants with the largest differences to STANDARD variant (dSTA)  
 2 regarding global freshwater fluxes (Q and AET) and total water storages trends (dTWS/dt)  
 3 (from Table 2, values in km<sup>3</sup> yr<sup>-1</sup>) as well as median  $E_{NS}$  for monthly time series of river  
 4 discharge at the 1319 calibration basins.

Variable	STANDARD	rank 1	dSTA	rank 2	dSTA	rank 3	dSTA
Q	40 458	NoCal	6364	CLIMATE	1906	NoUse	758
AET	69 803	NoCal	-6459	STRUCTURE	414	LANDCOVER	209
dTWS/dt	-214	STRUCTURE	169	NoUse	140	NoCal	71
median $E_{NS}$	0.54	NoCal	-0.66	STRUCTURE	-0.05	CLIMATE	-0.03

5

6

1 Table 7. Rank of model variants where global land area (except Greenland and Antarctica) is  
 2 affected most based on a threshold which represents the 10<sup>th</sup> percentile of averaged (1971-  
 3 2000) global grid cell values for AET and discharge.

rank	variant	% of area affected by changes	
		above 10 <sup>th</sup> percentile	
		AET	discharge
1	NoCal	60.5	13.5
2	CLIMATE	45.5	3.2
3	LANDCOVER	24.2	1.2
4	STRUCTURE	13.6	1.1
5	NoUse	0.9	0.03

4

5

1 Table A1. Parameters of the leaf area index model.

no.	land cover type	$L_{\max}$ [-]	fraction of deciduous plants $f_{d,lc}$	$L$ reduction factor for evergreen plants $c_{e,lc}$	initial days to start/end with growing season [d]
1	Evergreen needleleaf forest	4.02 <sup>a</sup>	0	1	1
2	Evergreen broadleaf forest	4.78 <sup>b</sup>	0	0.8	1
3	Deciduous needleleaf forest	4.63	1	0.8	10
4	Deciduous broadleaf forest	4.49 <sup>c</sup>	1	0.8	10
5	Mixed forest	4.34 <sup>d</sup>	0.25	0.8	10
6	Closed shrubland	2.08	0.5	0.8	10
7	Open shrubland	1.88	0.5	0.8	10
8	Woody savanna	2.08	0.5	0.3	10
9	Savanna	1.71	0.5	0.5	10
10	Grassland	1.71	0	0.5	10
11	Permanent wetland	6.34	0	0	10
12	Cropland	3.62	0	0.1	10
13	Cropland/ natural vegetation mosaic	3.62	0.5	0.5	10
14	Snow and ice	0	0	0	0
15	Bare ground	1.31	0	1	10

2 <sup>a</sup>  $L_{\max}$  is assumed to be the mean value of land cover classes of Scurlock et al. (2001) TeENL  
3 and BoENL, <sup>b</sup> only value for TrEBL and not TeEBL (Scurlock et al., 2001) as in WaterGAP  
4 this class is mainly in the tropics, <sup>c</sup> mean value from TeDBL and TrDBL (Scurlock et al.,  
5 2001), <sup>d</sup> mean value of all forest classes. Fraction of deciduous plants and  $L$  reduction factor  
6 for evergreen plants based on IMAGE (Alcamo et al., 1998), initial days to start/end with  
7 growing season are estimated.

1 Table A2. Attributes for IGBP land cover classes used in WaterGAP 2.2 for all model  
 2 variants, compiled from various literature sources. Water has an albedo of 0.08, snow 0.6.

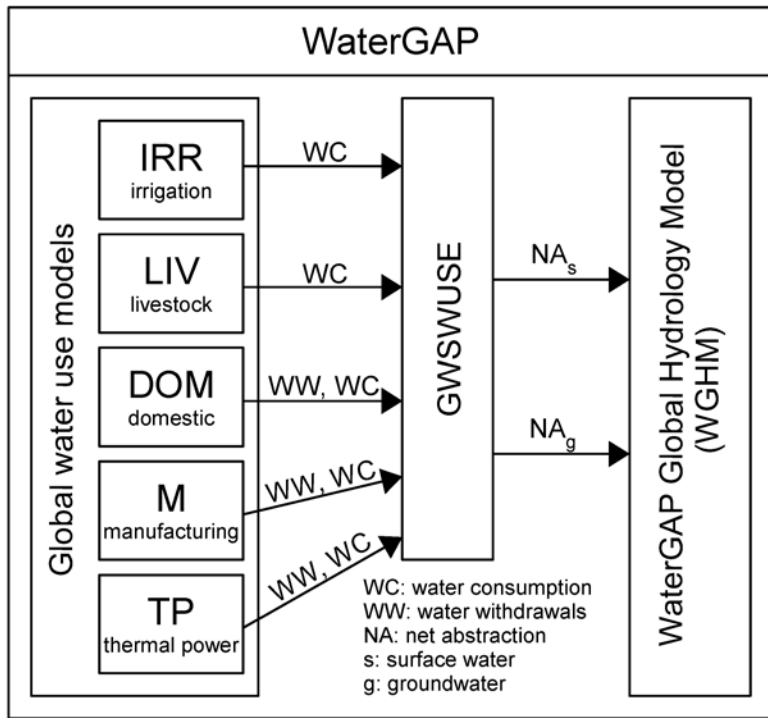
no.	land cover type	rooting depth <sup>a</sup> [m]	albedo <sup>a</sup> [-]	snow albedo [-]	emissivity <sup>b</sup> [-]	degree-day factor $D_F^c$ [mm d <sup>-1</sup> °C <sup>-1</sup> ]
1	Evergreen needleleaf forest	2	0.11	0.278	0.9956	1.5
2	Evergreen broadleaf forest	4	0.07	0.3	0.9956	3
3	Deciduous needleleaf forest	2	0.13	0.406	0.99	1.5
4	Deciduous broadleaf forest	2	0.13	0.558	0.99	3
5	Mixed forest	2	0.12	0.406	0.9928	2
6	Closed shrubland	1	0.13	0.7	0.9837	3
7	Open shrubland	0.5	0.2	0.7	0.9541	4
8	Woody savanna	1.5	0.2	0.558	0.9932	4
9	Savanna	1.5	0.3	0.7	0.9932	4
10	Grassland	1	0.25	0.7	0.9932	5
11	Permanent wetland	1	0.15	0.2	0.992	4
12	Cropland	1	0.23	0.376	0.9813	4
13	Cropland/ natural vegetation mosaic	1	0.18	0.3	0.983	4
14	Snow and ice	1	0.6	0.7	0.9999	6
15	Bare ground	0.1	0.35	0.7	0.9412	6

3 <sup>a</sup>adapted from the IMAGE model (Alcamo et al., 1998)

4 <sup>b</sup>(Wilber et al., 1999)

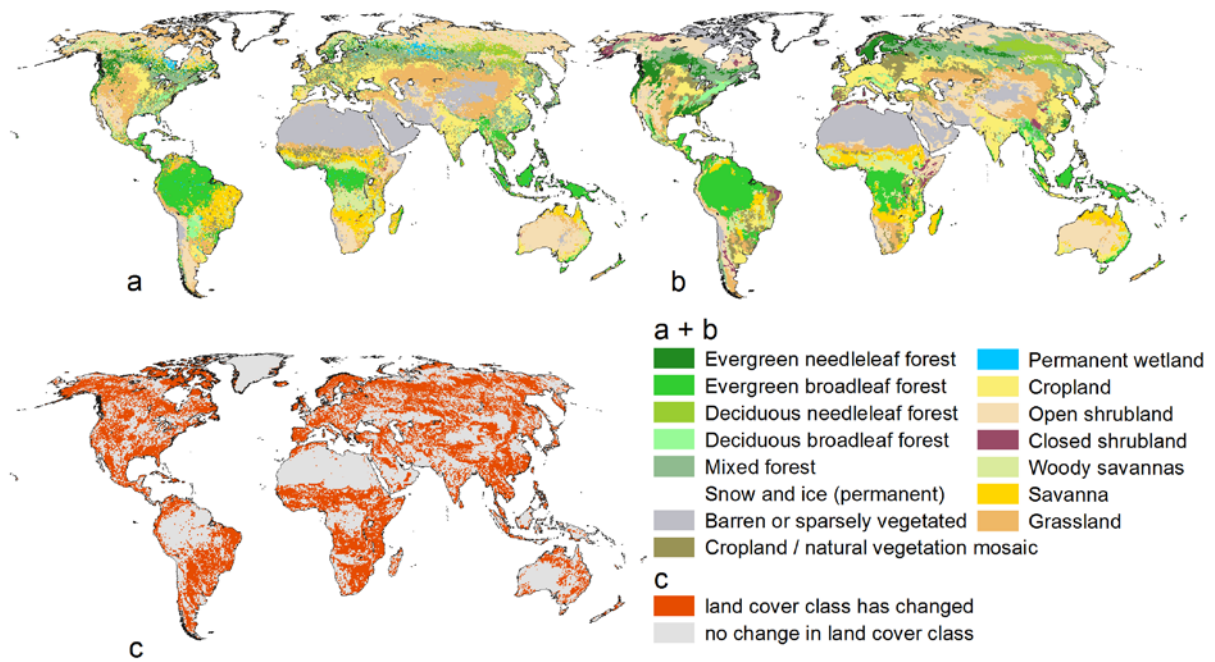
5 <sup>c</sup>(Maniak, 1997; WMO, 1994)

6



1  
 2 Figure 1. Schematic of WaterGAP 2.2. The output of five water use models is translated into  
 3 net abstractions from groundwater  $NA_g$  and surface water  $NA_s$  by the submodel GWSWUSE,  
 4 which allows computing the impact of human water use on water flows and storages by  
 5 WGHM. For details see Döll et al. (2012).  
 6

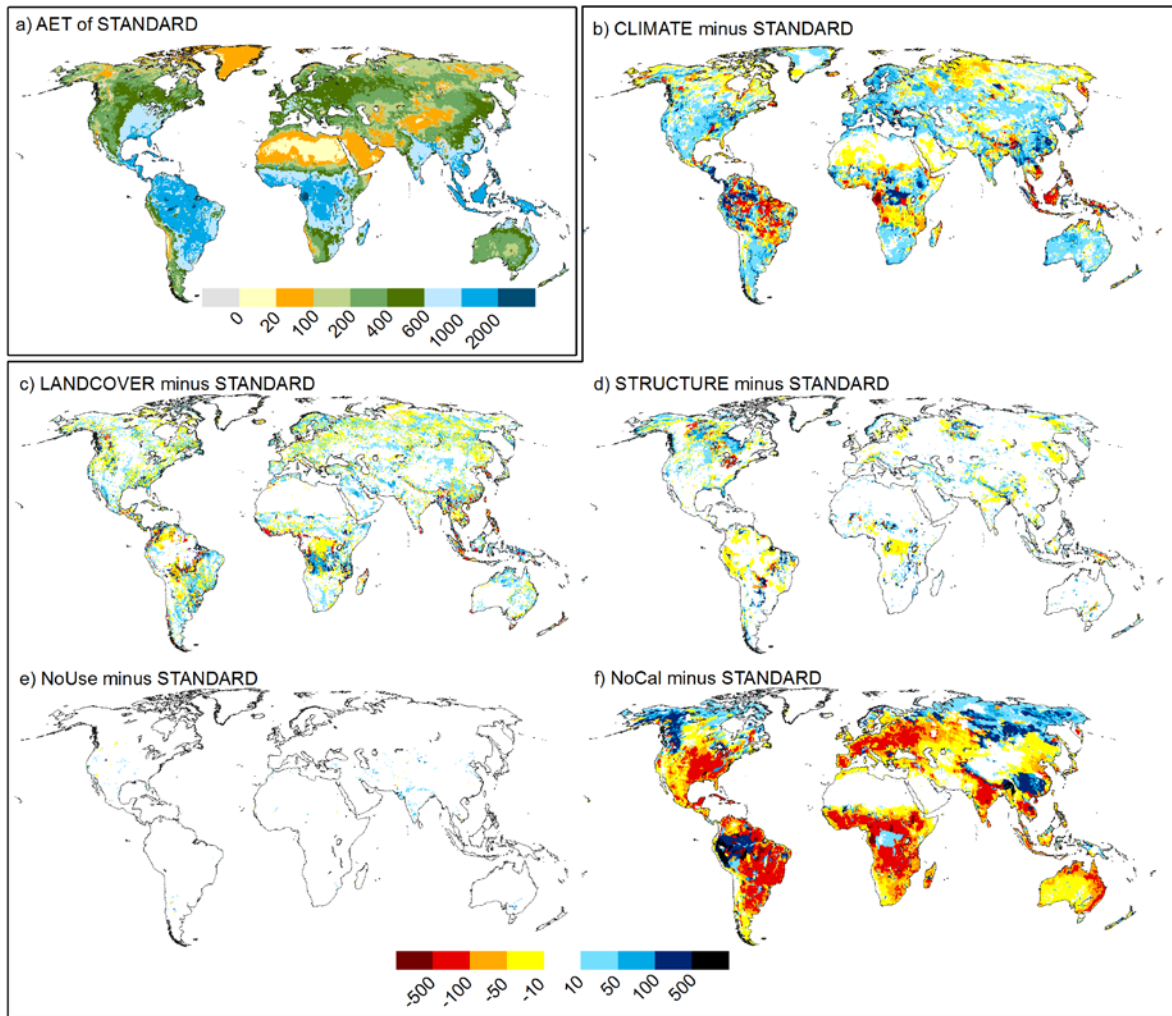




1

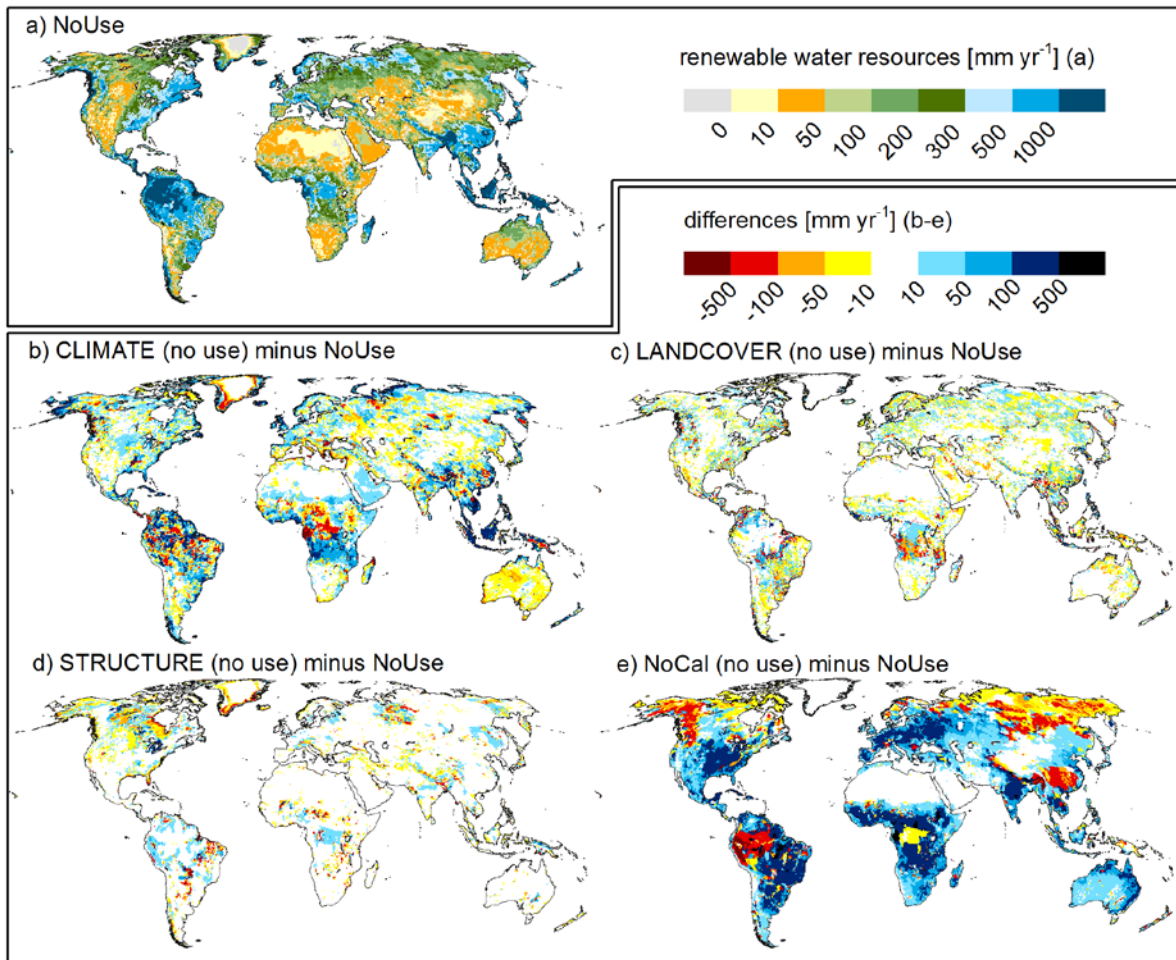
2 Figure 2. Land cover maps with a spatial resolution of 0.5° used as WaterGAP input based on  
 3 MODIS observations for the year 2004 (variant STANDARD) (a), land cover derived from  
 4 USGS GLCC but CORINE for Europe reflecting land cover distribution around the year 2000  
 5 (variant LANDCOVER) (b), and identification of grid cells where land cover class has  
 6 changed due to different input data (c).

7



1

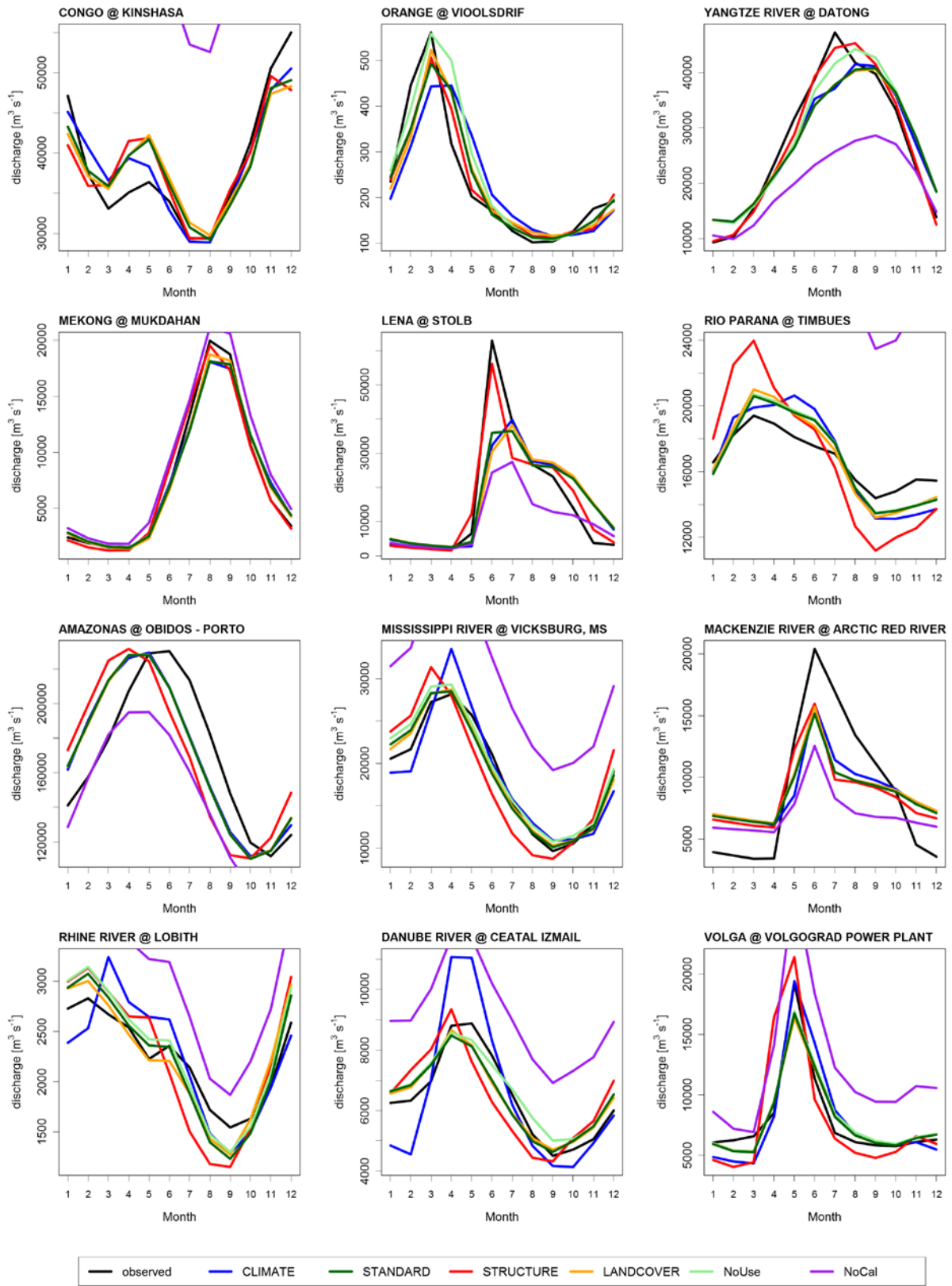
2 Figure 3. Actual evapotranspiration AET for STANDARD (mean value 1971-2000, in mm yr<sup>-1</sup>)  
 3 <sup>1</sup>) (a) and differences between the model variants and STANDARD in mm yr<sup>-1</sup> (b-f).  
 4



1

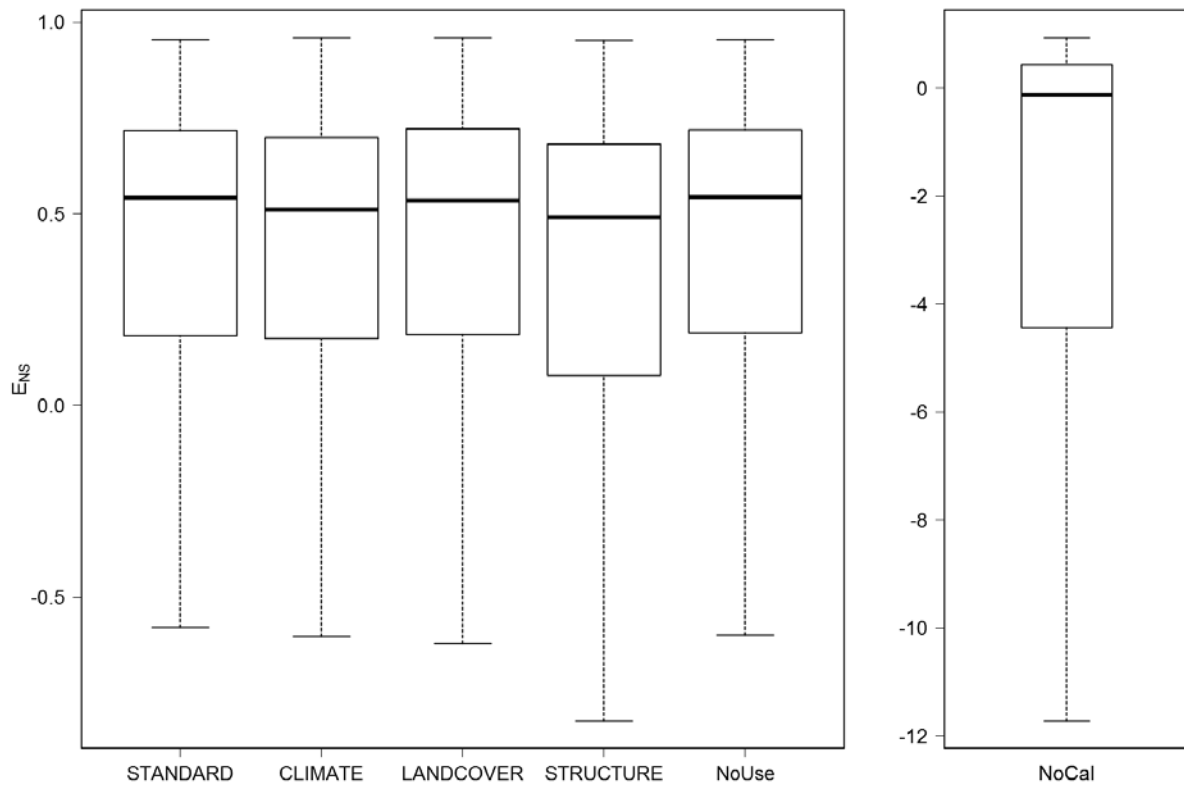
2 Figure 4. Renewable water resources (mean annual runoff from each cell if water use is  
 3 neglected) calculated by WaterGAP 2.2 NoUse variant (a) and differences to other variants  
 4 (variants here run without considering water use) (b-e).

5



1  
2  
3  
4

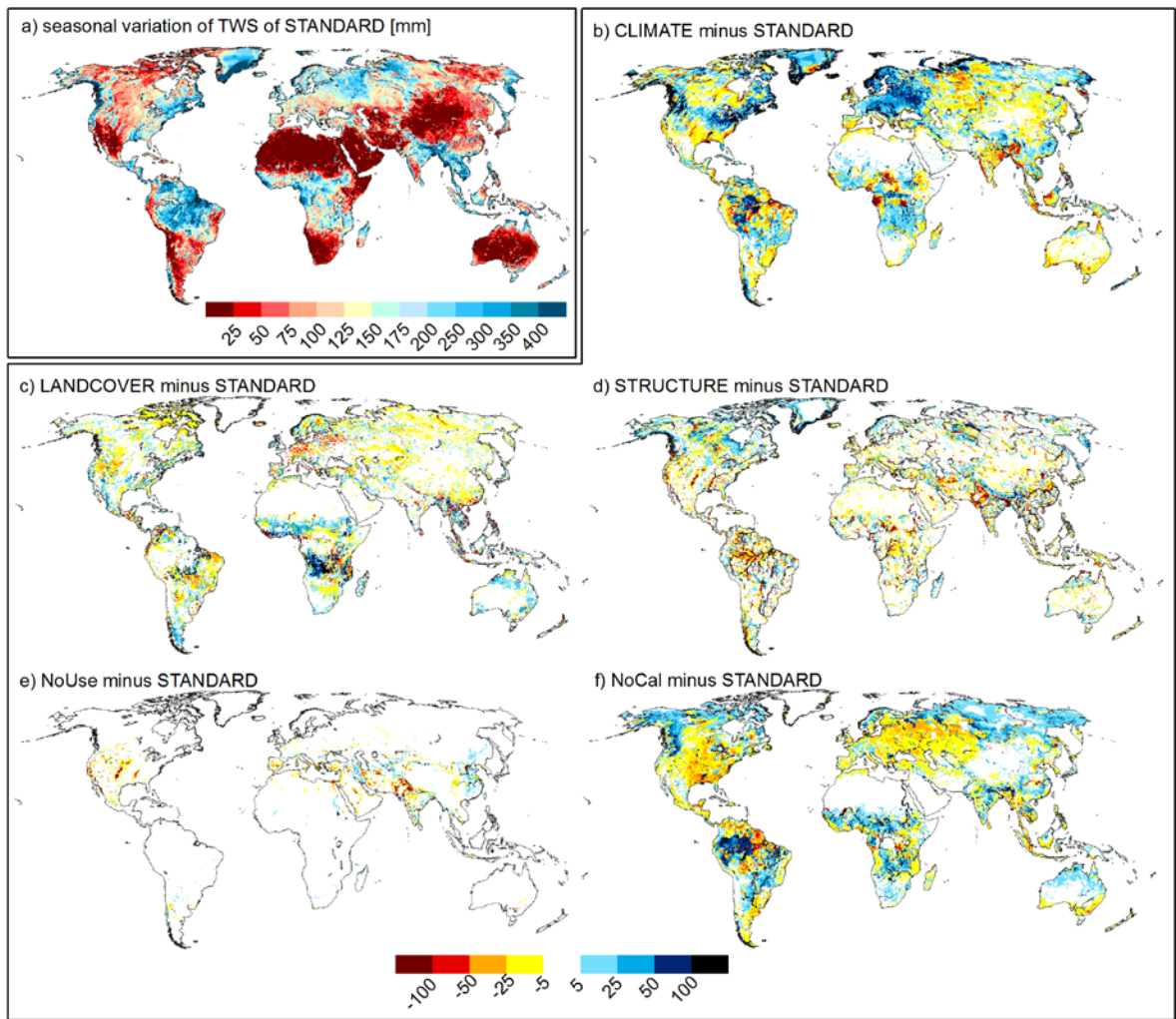
Figure 5. Discharge seasonality for selected basins and the calibrated model variants. Values for NoCal are only visible if they are in the range of calibrated model variants.



1

2 Figure 6. Nash-Sutcliffe efficiencies  $E_{NS}$  (excluding outliers) of monthly observed and  
 3 simulated discharge at 1319 stations used for calibration.

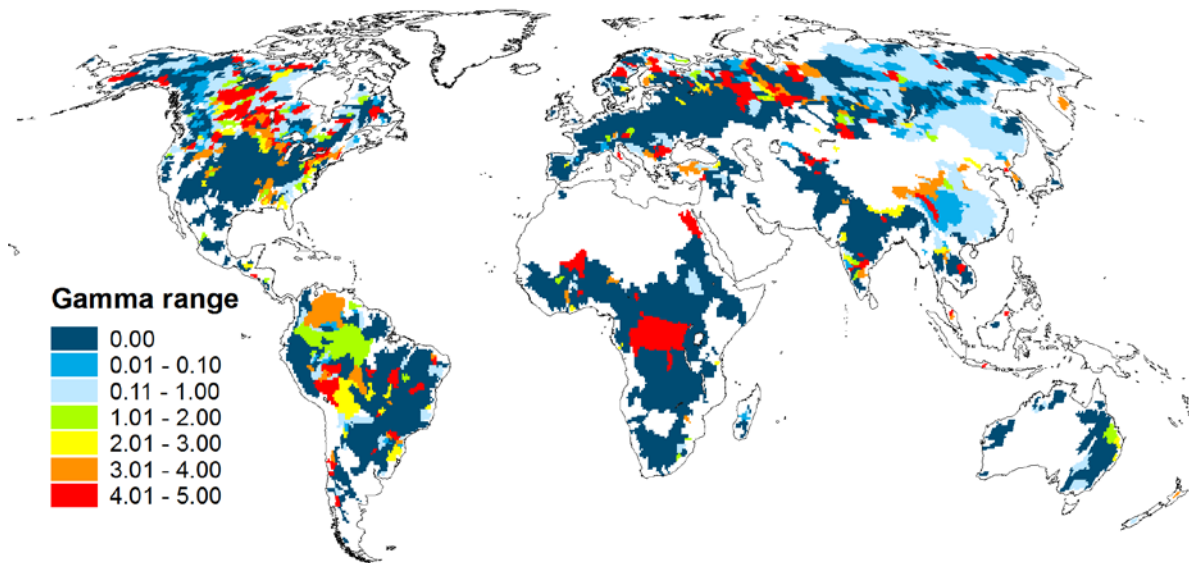
4



1

2 Figure 7. Seasonal variation of total water storage (TWS) for STANDARD (a) and as  
 3 difference maps [mm] to all other model variants (b-f).

4

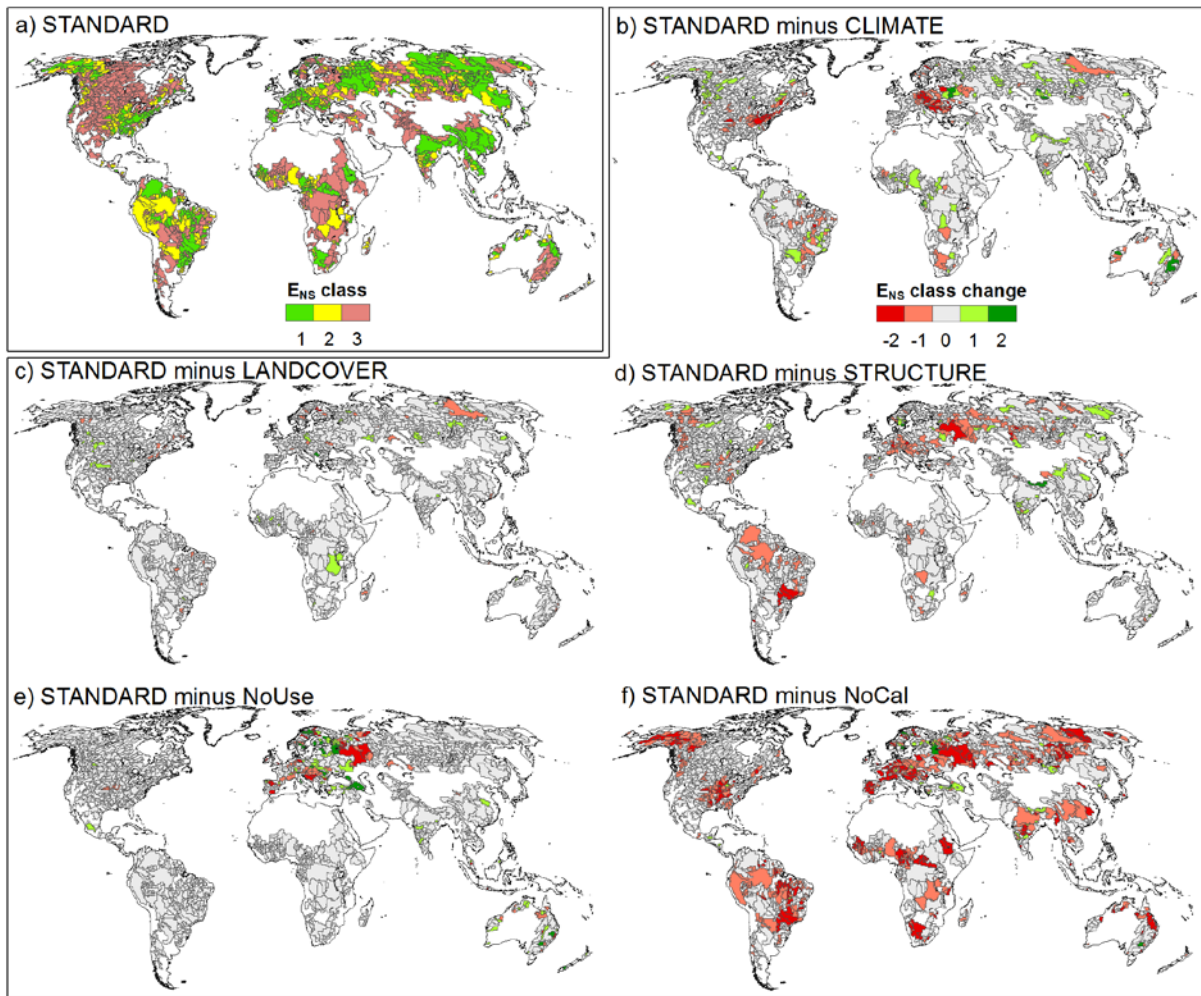


1

2 Figure 8. Range of calibration parameter  $\gamma$  through all four calibrated model variants  
3 (calculated as  $\gamma_{\max} - \gamma_{\min}$ ) showing the general sensitivity to input data and model structure.

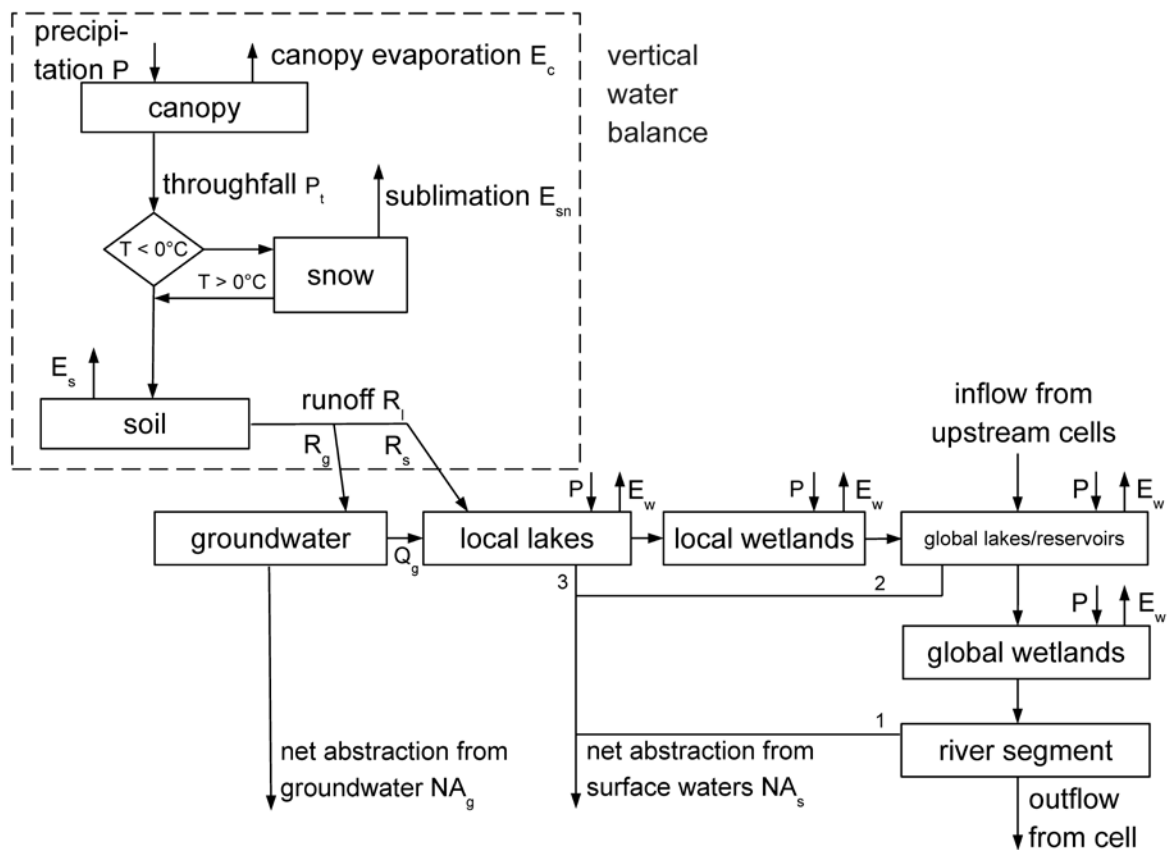
4 White colors indicate uncalibrated regions.

5



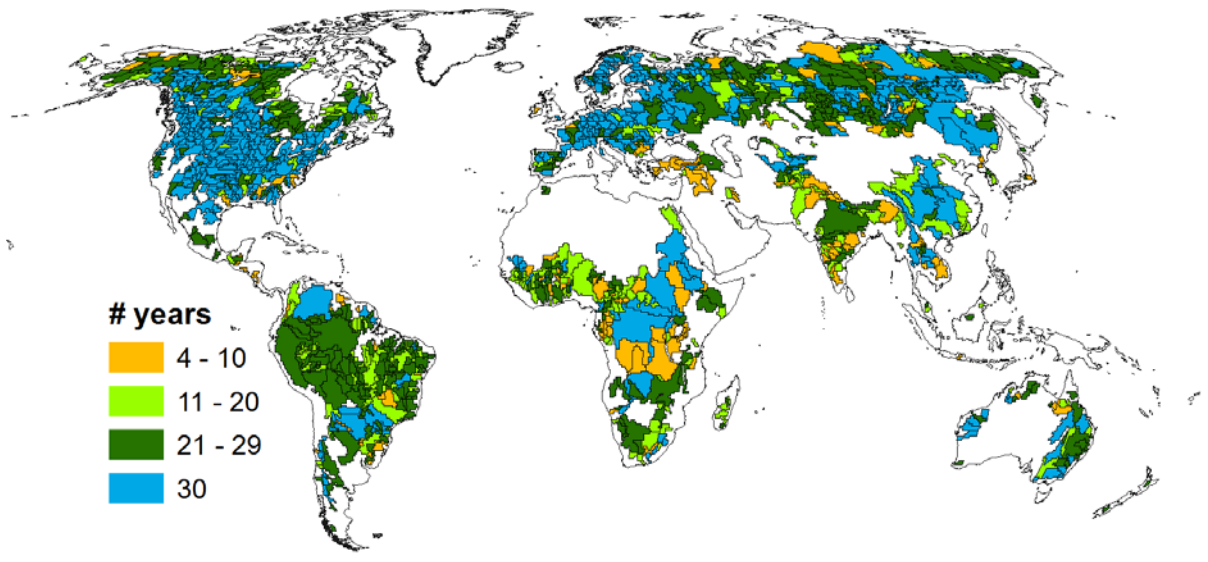
1  
2 Figure 9. Spatial distribution of Nash-Sutcliffe efficiency  $E_{NS}$  classes (from Table 4, 1:  $E_{NS}$   
3  $> 0.7$ , 2:  $0.5 < E_{NS} < 0.7$ , 3:  $E_{NS} < 0.5$ ) for STANDARD (a), and differences of model  
4 variants (calculated as STANDARD  $E_{NS}$  class minus that of the model variant) (b-f). Red  
5 colors indicate a decrease, green an increasing  $E_{NS}$  when using the model variant compared  
6 to STANDARD.  
7





1  
2  
3  
4  
5  
6  
7

Figure A1. Schematic structure of the water fluxes and storages as computed by WaterGAP Global Hydrology Model (WGHM) within each  $0.5^\circ$  grid cell. Boxes represent water storage compartments, arrows water fluxes (inflows, outflows). Numbers at net abstraction from surface waters ( $NA_s$ ) are the order from which storage water is abstracted until demand is satisfied.



1

2 Figure B1. Calibration basins of WaterGAP 2.2 with number of years with discharge  
3 observations used for calibration.

4